



113
927
THS



This is to certify that the

thesis entitled

AGING EFFECTS AND PHASE TRANSFORMATIONS
IN A $Ti_{49.5}Ni_{48}Cr_{2.5}$ ALLOY

presented by

Chulsoo Kim

has been accepted towards fulfillment
of the requirements for

Master degree in Materials Science

C. M. Young
Major professor

Date 5/16/86



RETURNING MATERIALS:
Place in book drop to
remove this checkout from
your record. FINES will
be charged if book is
returned after the date
stamped below.

--	--	--

AGING EFFECTS AND PHASE TRANSFORMATIONS
IN A $\text{Ti}_{49.5}\text{Ni}_{48}\text{Cr}_{2.5}$ ALLOY

BY

Chulsoo Kim

A THESIS

Submitted to
Michigan State University
in partial fulfillment of the requirements
for the degree of

MASTER OF SCIENCE

Department of Metallurgy, Mechanics and Materials Science

1986

ABSTRACT

AGING EFFECTS AND PHASE TRANSFORMATIONS
IN A $\text{Ti}_{49.5}\text{Ni}_{48}\text{Cr}_{2.5}$ ALLOY

BY

Chulsoo Kim

The transformation behavior and the effects of aging on the transformation temperatures in a $\text{Ti}_{49.5}\text{Ni}_{48}\text{Cr}_{2.5}$ alloy have been studied using electrical resistance measurements between room temperature and -196°C .

Transmission electron microscopy and electron diffraction studies were performed at ambient temperature and in-situ cooling experiments were carried out in a scanning transmission electron microscope between room temperature and -136°C . Based on the results obtained, the $\text{Ti}_{49.5}\text{Ni}_{48}\text{Cr}_{2.5}$ alloy exhibits the charge density wave (CDW) phenomena similar to TiNiFe and TiNiAl alloys.

The aging treatments decrease the M_s , A_s , and A_f temperatures up to a certain period of aging and then increase them after that. This effect was attributed to the formation of Ti-rich precipitates.

The alloy was cycled thermally and was little affected even after 50 cycles. The M_s temperature was increased by cold-rolling and returned to the as-annealed value after aging treatment.

ACKNOWLEDGEMENTS

I should express my sincerest thanks to my parents for their never ending love and support. I wish to thank to Dr. C. M. Hwang for his advice and guidance. I am also indebted to Mr. Shull Vivon, from Physics department, who helped in using the STEM. Thanks are due to Ms. Patricia Dodge for her careful reading and valuable correction. Finally, special thanks to Raychem Co. for their supply of the material.

TABLE OF CONTENTS

	Page
LIST OF TABLES	iv
LIST OF FIGURES	v
I. INTRODUCTION	1
II. EXPERIMENTAL PROCEDURE	8
III. RESULTS AND DISCUSSION	10
IV. SUMMARY	67
LIST OF REFERENCES	68

LIST OF TABLES

Table	Page
I. Transformation temperatures of the as-annealed and thermal-cycled $\text{Ti}_{49.5}\text{Ni}_{48}\text{Cr}_{2.5}$ alloy	14
II. The effect of aging on the transformation temperatures of the $\text{Ti}_{49.5}\text{Ni}_{48}\text{Cr}_{2.5}$ alloy . .	23
III. Transformation temperatures of the $\text{Ti}_{49.5}\text{Ni}_{48}\text{Cr}_{2.5}$ alloy, cold-rolled and cold-rolled followed by aging	61

LIST OF FIGURES

Figure	Page
1. Electrical resistance vs. temperature curve for the as-annealed $\text{Ti}_{49.5}\text{Ni}_{48}\text{Cr}_{2.5}$ alloy	11
2. Electrical resistance vs. temperature curve for the 50th full thermal-cycled specimen	12
3. Transmission electron micrograph and corresponding diffraction patterns of the parent phase of the $\text{Ti}_{49.5}\text{Ni}_{48}\text{Cr}_{2.5}$ alloy taken at room temperature. (a) Bright field image (x50,000); (b) $[111]_{\text{B}_2}$ zone diffraction pattern; (c) $[110]_{\text{B}_2}$ zone diffraction pattern	15
4. Transmission electron micrographs and corresponding diffraction pattern of the $\text{Ti}_{49.5}\text{Ni}_{48}\text{Cr}_{2.5}$ alloy taken at room temperature. (a) Bright field image (x40,000); (b) $[111]_{\text{B}_2}$ zone diffraction pattern; (c) Dark field image (x40,000)	18
5. Scanning transmission electron micrograph taken at -136°C and corresponding diffraction patterns taken at -136°C and room temperature. (a) Bright field image (x50,000); (b) Selected area diffraction pattern taken at -136°C ; (c) $[110]_{\text{B}_2}$ zone diffraction pattern taken at room temperature	20
6. Electrical resistance vs. temperature curve for the $\text{Ti}_{49.5}\text{Ni}_{48}\text{Cr}_{2.5}$ alloy aged at 400°C . (a) aged for 5 min.; (b) aged for 30 min.; (c) aged for 1 hr.; (d) aged for 4 hrs.; (e) aged for 12 hrs.; (f) aged for 24 hrs.	24
7. Transmission electron micrographs of the $\text{Ti}_{49.5}\text{Ni}_{48}\text{Cr}_{2.5}$ alloy aged at 400°C . (a) Bright field image (x60,000), aged for 1 hr.; (b) Bright field image (x60,000), aged for 4 hrs.; (c) Bright field image (x60,000), aged for 12 hrs.	31

LIST OF FIGURES (Continued)

Figure	Page
8. Electrical resistance vs. temperature curve for the $Ti_{49.5}Ni_{48}Cr_{2.5}$ alloy aged at 500 °C. (a) aged for 5 min.; (b) aged for 30 min.; (c) aged for 1 hr.; (d) aged for 4 hrs.; (e) aged for 12 hrs.; (f) aged for 24 hrs.34
9. Transmission electron micrographs of the $Ti_{49.5}Ni_{48}Cr_{2.5}$ alloy aged at 500 °C. (a) Bright field image (x150,000), aged for 1 hr.; (b) Bright field image (x150,000), aged for 4 hrs.; (c) Bright field image (x150,000), aged for 12 hrs.41
10. Electrical resistance vs. temperature curve for the $Ti_{49.5}Ni_{48}Cr_{2.5}$ alloy aged at 600 °C. (a) aged for 5 min.; (b) aged for 30 min.; (c) aged for 1 hr.; (d) aged for 4 hrs.; (e) aged for 12 hrs.; (f) aged for 24 hrs.43
11. Transmission electron micrographs and selected area diffraction pattern of the $Ti_{49.5}Ni_{48}Cr_{2.5}$ alloy aged at 600 °C. (a) Bright field image (x150,000), aged for 1 hr.; (b) Bright field image (x150,000), aged for 4 hrs.; (c) Bright field image (x150,000), aged for 24 hrs.; (d) $[211]_{B2}$ zone diffraction pattern; (e) Dark field image (x150,000), aged for 24 hrs.49
12. Variation of the transformation temperatures vs. aging time at various temperatures. (a) Variation of M_s temperature vs. aging time; (b) Variation of A_s temperature vs. aging time; (c) Variation of A_f temperature vs. aging time; (d) Variation of T_p temperature vs. aging time; (e) Variation of T_d temperature vs. aging time	53

LIST OF FIGURES (Continued)

Figure	Page
13. Electrical resistance vs. temperature curve for the $\text{Ti}_{49.5}\text{Ni}_{48}\text{Cr}_{2.5}$ alloy, 20% cold-rolled. . .	59
14. Electrical resistance vs. temperature curve for the $\text{Ti}_{49.5}\text{Ni}_{48}\text{Cr}_{2.5}$ alloy, 20% cold-rolled followed by aging at 500 °C for 4 hrs.60
15. Transmission electron micrographs and corresponding diffraction patterns of $\text{Ti}_{49.5}\text{Ni}_{48}\text{Cr}_{2.5}$ alloy, 20% cold-rolled. (a) Bright field image (x50,000); (b) $[122]_{\text{B}2}$ zone diffraction pattern; (c) $[122]_{\text{B}2}$ and $[\bar{1}\bar{1}\bar{1}]_{\text{B}19}$ zone diffraction pattern; (d) Dark field image (x60,000)62
16. Transmission electron micrographs of the $\text{Ti}_{49.5}$ $\text{Ni}_{48}\text{Cr}_{2.5}$ alloy, 20% cold-rolled followed by aging at 500 °C for 4 hrs. (a) Bright field image (x20,000) ; (b) Bright field image (x60,000)	66

I. Introduction

TiNi with nearly equiatomic composition has received considerable attention because of its peculiar shape memory effect and premartensitic anomalous phenomena. The shape memory effect can be described as follows. An object in the low temperature martensitic condition, (usually below M_f) when it is deformed, and the stress then removed, will regain its original shape when heated above the A_s temperature. The process of regaining the original shape is associated with the reverse transformation of the deformed martensitic phase.

The number of materials exhibiting the shape memory effects is now extensive. The lists includes the binary TiNi alloys (Nitinol), ternary TiNiX alloys, many Cu-based alloys, noble metal (Au, Ag)-based alloys, Ni-Al alloys and Fe-Pt alloys. Among these alloys that exhibit shape memory effect TiNi type alloys were reported to have the best combination of physical and mechanical properties.

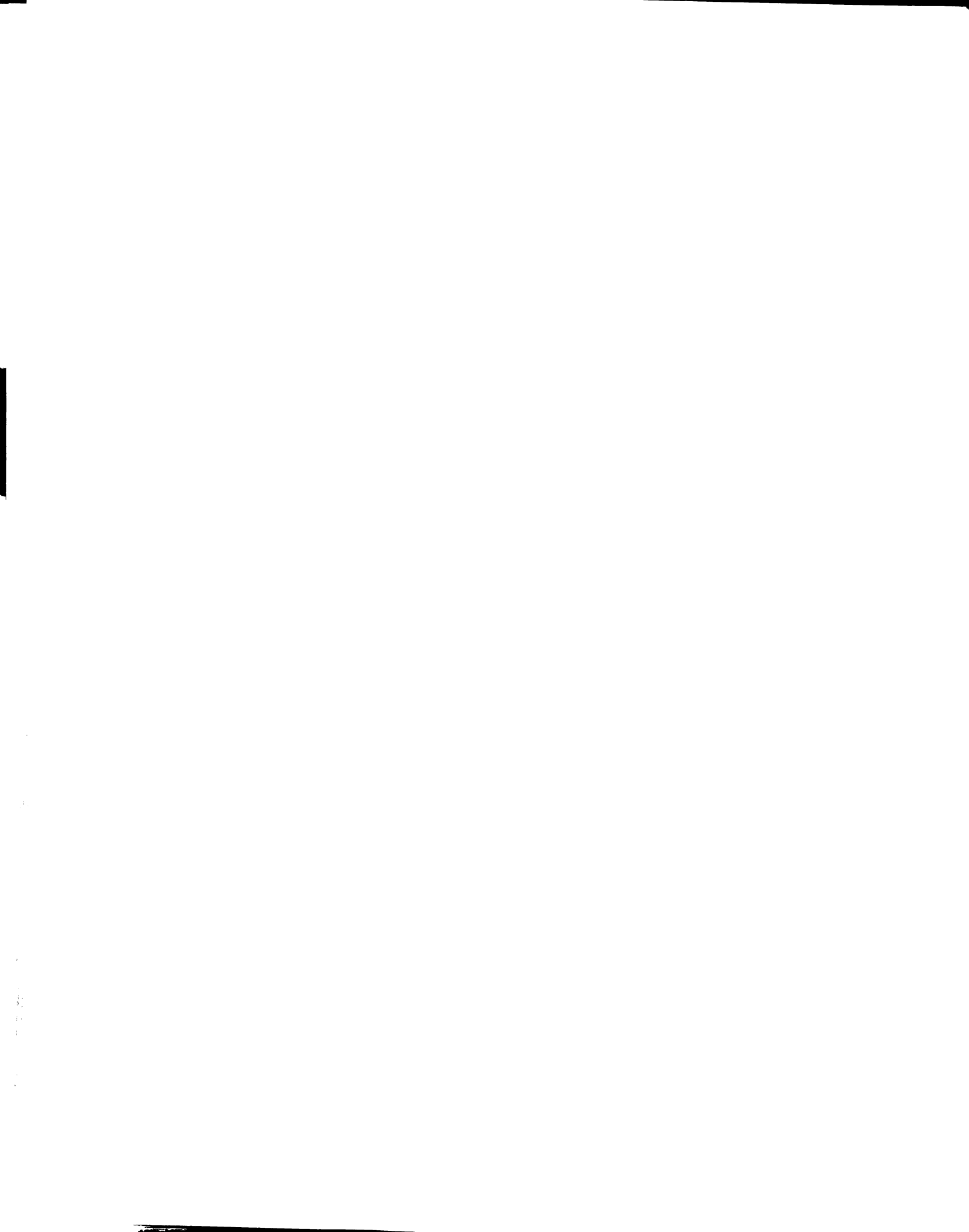
Wayman and Shimizu (1) first suggested the necessary conditions for the shape memory effect as follows. The martensites formed thermoelastically, are either internally twinned or internally faulted as a consequence of the inhomogeneous shear process, and the parent phase is ordered.

A thermoelastic martensitic transformation is defined as one in which the martensite forms and grows continuously

as the temperature is lowered, and shrinks and vanishes continuously as the temperature is raised.

It has been reported that the martensitic transformation in TiNi exhibits 'premartensitic phenomena' immediately above the martensitic start temperature. These include an electrical resistivity increase, streaks in the electron diffraction patterns, and $1/3$ spots in both electron and X-ray diffraction patterns. Other anomalies in physical and mechanical properties have also been reported such as an unusual high damping capacity, internal friction peaks, a decrease in sound velocity, a softening of certain elastic moduli and specific heat peaks. These premartensitic phenomena were interpreted earlier as precursory effects closely related with the martensitic phase transformation. However, after many investigations by a number of workers, it was shown that TiNi alloys undergo a characteristic premartensitic transition in addition to the martensitic transformation. The crystal structure of the phase produced by the premartensitic transformation was reported to be rhombohedral by Dautovich and Purdy (2). Ling and Kaplow (3) referred the phase associated with premartensitic behaviour as the 'R phase'.

Many investigators have also discussed the premartensitic phenomena. Chandra and Purdy (4) observed the diffuse scattering of electrons in TiNi foils and they interpreted in terms of kinematical scattering from large amplitude, short wavelength phonons. Sandrock et al. (5)



noticed the formation of $\{111\}$ planes of diffuse intensity in reciprocal space well above the M_s temperature. They discussed the premartensitic phenomena in terms of lattice vibrations reflecting an incipient mechanical instability of the B2 lattice and proposed that the origin of the instability presumably lies in bonding (electronic) changes.

Otsuka et al.(6) using electron diffraction found the $1/3$ reflections and they speculated that the transition may be either an electronic ordering or a lattice modulation due to periodic displacements of atoms. Several years ago, Moine et al. (7) also studied the premartensitic effects in TiNi by using electron diffraction and various transmission electron microscopy imaging techniques. They observed an extensive array of the extra spots in the electron diffraction patterns and interpreted it as lattice displacement waves (LDW) in the structure.

Most recently, using ternary TiNiFe and TiNiAl alloys, it was proposed that three-dimensional charge density wave (CDW) phenomena and associated phase transitions are involved in the premartensitic behavior of the TiNi type alloys (8-16). Two premartensitic transitions are suggested. The first premartensitic transition is a second order ' normal-to-incommensurate' transition and in this stage the positions of the $1/3$ superlattice reflections in the electron diffraction patterns are deviated slightly from the exact $1/3$ positions. Antiphase-like microdomains (APD's)

were revealed in dark-field images using the deviated 1/3 reflections.

A second premartensitic transition, which occurs at a lower temperature (T_d), is a first order 'incommensurate-to-commensurate' transformation and the positions of 1/3 superlattice reflections are at exact 1/3 positions. At below T_d , needle domains were observed.

Thus, the sequence of transformations (upon cooling) in the TiNiFe and TiNiAl alloys is as follows:

parent phase (B2) - incommensurate phase (distorted cubic) - commensurate phase (rhombohedral) - martensitic phase (monoclinic).

A charge density wave (CDW) is a static modulation of conduction electrons and is a Fermi-surface driven phenomenon usually accompanied by a periodic lattice distortion. Numerous examples of a CDW phase change have been found in quasi-one-dimensional organic conductors (e.g. TTF-TCNQ) and quasi-two-dimensional layered compounds (e.g. transition-metal dichalcogenides) (16-18).

A favorable Fermi surface geometry is necessary for the formation of a CDW which will most likely occur when the shape of the Fermi surface permits a connection by the same wave vector Q , ie. $Q = 2 K_f$. This modulation with wave vector Q will modify the Fermi surface by creating gaps at these nested positions. If the nested portion of the Fermi surface is significant the energy gain by creating energy gaps may overcome the energy cost arising from the periodic

lattice distortions, thus allowing the formation of a CDW.

Another requirement for forming a CDW is a strong electron-phonon coupling. This permits ion displacements to reduce the prohibitive coulomb energy. Precursor phenomena, such as a soft phonon mode, might also occur above the transition temperature to assist the CDW instability.

Since a CDW is accompanied by a lattice distortion, diffraction techniques (electron, neutron, X-ray) can be used to reveal satellite reflections appearing near the Bragg reflections of the parent phase as a consequence of the formation of the CDW. These reflections are separated from the associated Bragg reflections by a reciprocal lattice vector determined by the CDW wave vector.

Honma et al. (19) studied the effects of 3d transition elements (V, Cr, Mn, Fe and Co) on the phase transformation in TiNi alloy and concluded that M_s point decreases as the valence electron concentration (e/a) deviates from the seven in those ternary alloys. It was also reported that the decreasing rate of the M_s point was larger than that of the premartensitic transition temperature.

Thus the ternary $Ti_{49.5}Ni_{48}Cr_{2.5}$ alloy, which was used in this present study, is expected to be ideal for studying the premartensitic transition. As previously mentioned, the premartensitic transition in the TiNiFe and TiNiAl alloys are believed to be associated with the formation of three-dimensional charge density wave. Therefore, one of the main purpose of the present investigation is to see whether



the $\text{Ti}_{49.5}\text{Ni}_{48}\text{Cr}_{2.5}$ alloy undergoes the charge density wave transition.

In a practical point a view, it seems to be important to investigate the effect of thermo-mechanical treatments on the transformation behavior and the shape memory effects in the various shape memory alloys.

Saburi et al. (20) investigated the aging effects on the transformation temperatures and the deformation behavior of Ni-rich Ti-Ni alloys with different Ni contents. They found that M_s temperature and mechanical behavior of Ni-rich off-stoichiometric Ti-Ni alloys were sensitive to heat-treatment, while those of a near-stoichiometric alloys were not.

Recently, Nishida and Honma (21) discovered an excessive reversible shape memory effect, which was dubbed as an 'all-round shape memory effect (ARSME)', in Ni-rich TiNi alloys by constrained aging treatment and proposed that this phenomena was ascribed to the formation of widmanstatten lenticular precipitates with two variants. Further studies were carried out by Nishida et al. (22) using transmission electron microscopy and EDX microanalytical system. It was confirmed that the composition of the precipitate was $\text{Ti}_{11}\text{Ni}_{14}$ and the structure of the $\text{Ti}_{11}\text{Ni}_{14}$ can be explained as monoclinic.

In general, the M_s temperature depends on the chemical composition, hydrostatic stress, lattice defects (vacancy, dislocation, precipitate and grain boundary) and external

shear stress (23). In the case of TiNi type alloys , it has been reported that the Ms temperature is strongly dependent on the alloy composition.

The present study was undertaken to investigate the transformation behavior and the effects of aging on the transformation temperatures in a $\text{Ti}_{49.5}\text{Ni}_{48}\text{Cr}_{2.5}$ alloy. The effects of thermal cycling and cold-rolling on the transformation temperatures were also examined.



II. Experimental procedure

The alloy composition used for the present study was 49.5 at% Ti, 48 at% Ni and 2.5 at% Cr. The rod, which was approximately 14.7 mm in diameter, was cut into the 0.3 mm thick slices using a diamond saw. The samples were mechanically polished to a thickness of 0.1 mm by using SiC paper, and the discs, 3 mm in diameter, were sectioned for the transmission electron microscopy investigation.

The strip samples for electrical resistance measurements were also cut using a diamond saw and the final dimensions of the strips were approximately 34.8 mm in length, 1.5 mm in width and 0.4 mm in thickness.

All the samples were annealed at 950 °C for 2hrs. in a evacuated quartz tube and then quenched into cold water, breaking the quartz tube. They were sealed again and aged at 400 °C, 500 °C and 600 °C for different aging times between 5 min. to 24 hrs., and then water-quenched, breaking the quartz tube. Some specimens were 20% cold-rolled after the annealing treatment and some were aged at 500 °C for 4hrs., then water quenched.

Thin foils for TEM observations were made by a Tenupol-2 twin jet polishing machine equipped with the constant voltage supply (Polipower) and photo cell. An electrolyte, containing 92% glacial acetic acid and 8% perchrolic acid (70% conc.) by volume, was used at 15 °C under an applied potential of about 20 Volts. Electron

diffraction and TEM observations were carried out in a Hitachi H-800 microscope at room temperature, operated at 200 KV and equipped with a $\pm 60^\circ$ tilting stage. In-situ cooling experiment was performed in a V.G. HB 501 scanning transmission electron microscope between room temperature and -136°C , operated at 100 KV. The samples for electrical resistance measurements were electropolished after heat treatment to remove the oxidized surface. The same electrolyte was used at about 25 Volts.

A continuous measurement of electrical resistance as a function of temperature was achieved by means of an omnigraphic 200 X-Y recorder with a fast response time (24).

The liquid nitrogen vapor in a deep, wide mouth Dewar Vessel was used for a cooling medium. The cooling, or heating, rate of the specimen was approximately $0.6^\circ\text{C}/\text{sec}$. Four copper leads were spot welded to the ends of the sample ; outer two for current supply and inner two for potential measurement. A copper-constantan thermocouple was spot welded to the center of the specimen.

A regulated d.c. power supply served as a current source. One hundred and forty Volts was applied across the specimen with a current of approximately 140 mA. The specimen was lowered into the cooling bath by engaging a stepping motor, and raised by activation of a microswitch.

III. Results and Discussion

Transformation behavior

The electrical resistance versus temperature curve, obtained during a full thermal cycle between room temperature and liquid nitrogen temperature, for the as-annealed $\text{Ti}_{49.5}\text{Ni}_{48}\text{Cr}_{2.5}$ alloy is shown in Fig.1. It can be seen that the overall shape of the curve is analogous to that of TiNiFe and TiNiAl alloys which undergo the charge density wave transition.

Upon cooling the resistance starts to increase at T_p , which corresponds to the onset of the first premartensitic transition. The second premartensitic transformation begins at T_d where the curve seems to show an inflection point. At the M_s temperature the resistance starts to decrease until liquid nitrogen temperature, which is approximately the M_f temperature.

Upon heating, the resistance begins to increase slowly and then rises abruptly at the austenite start temperature (A_s). A small hysteresis can be found between A_f and T_p .

In Fig.2, the electrical resistance vs. temperature plot for the 50th full thermal cycled specimen is shown. It can be considered that the effects of thermal cycling on both the transformation temperatures and the shape of the electrical resistance vs. temperature curve are not significant in the $\text{Ti}_{49.5}\text{Ni}_{48}\text{Cr}_{2.5}$ alloy. Transformation temperatures of the as-annealed and the thermally-cycled

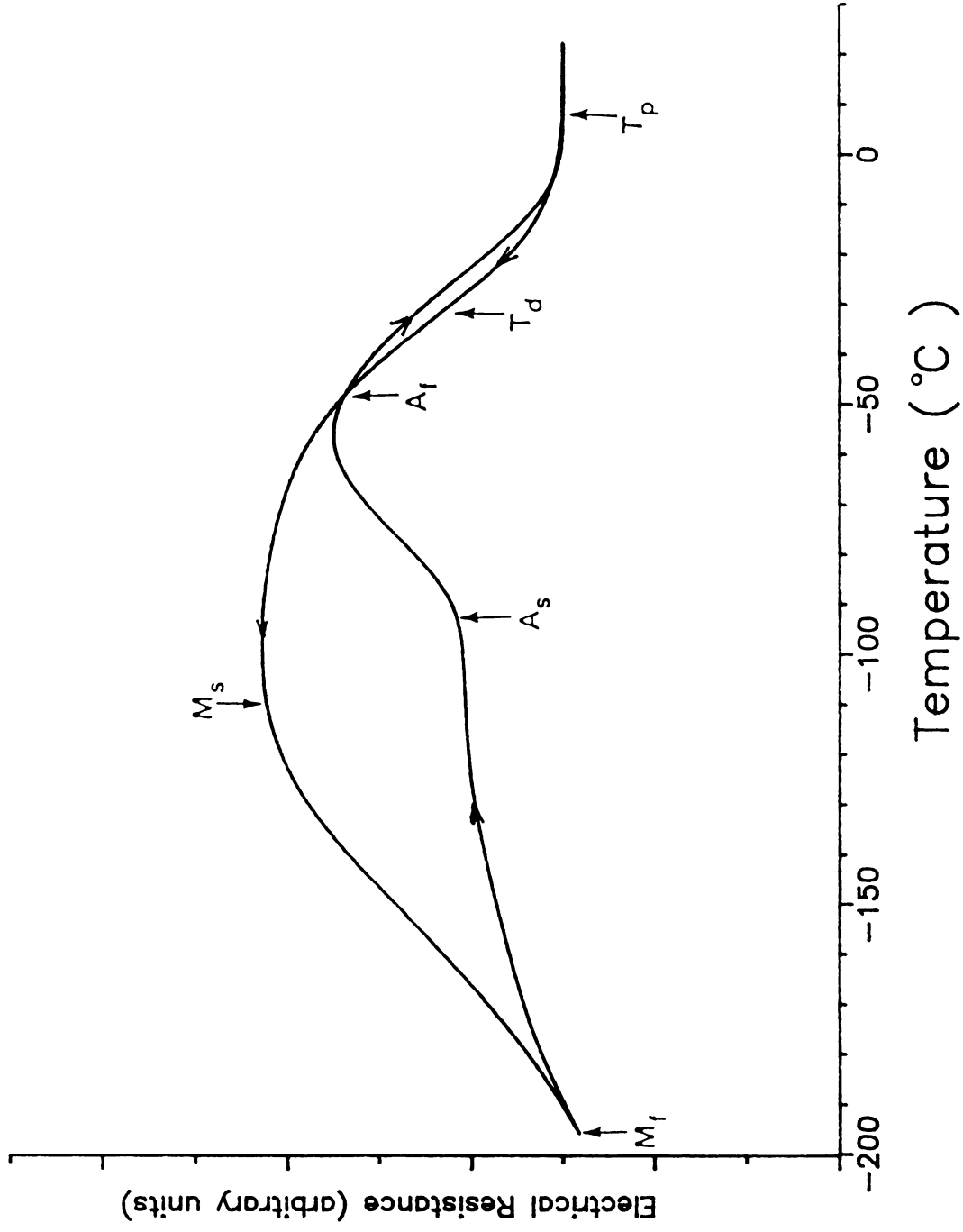


Fig 1. Electrical resistance vs. temperature curve for the as-annealed $Ti_{49.5}Ni_{48}Cr_{2.5}$ alloy.

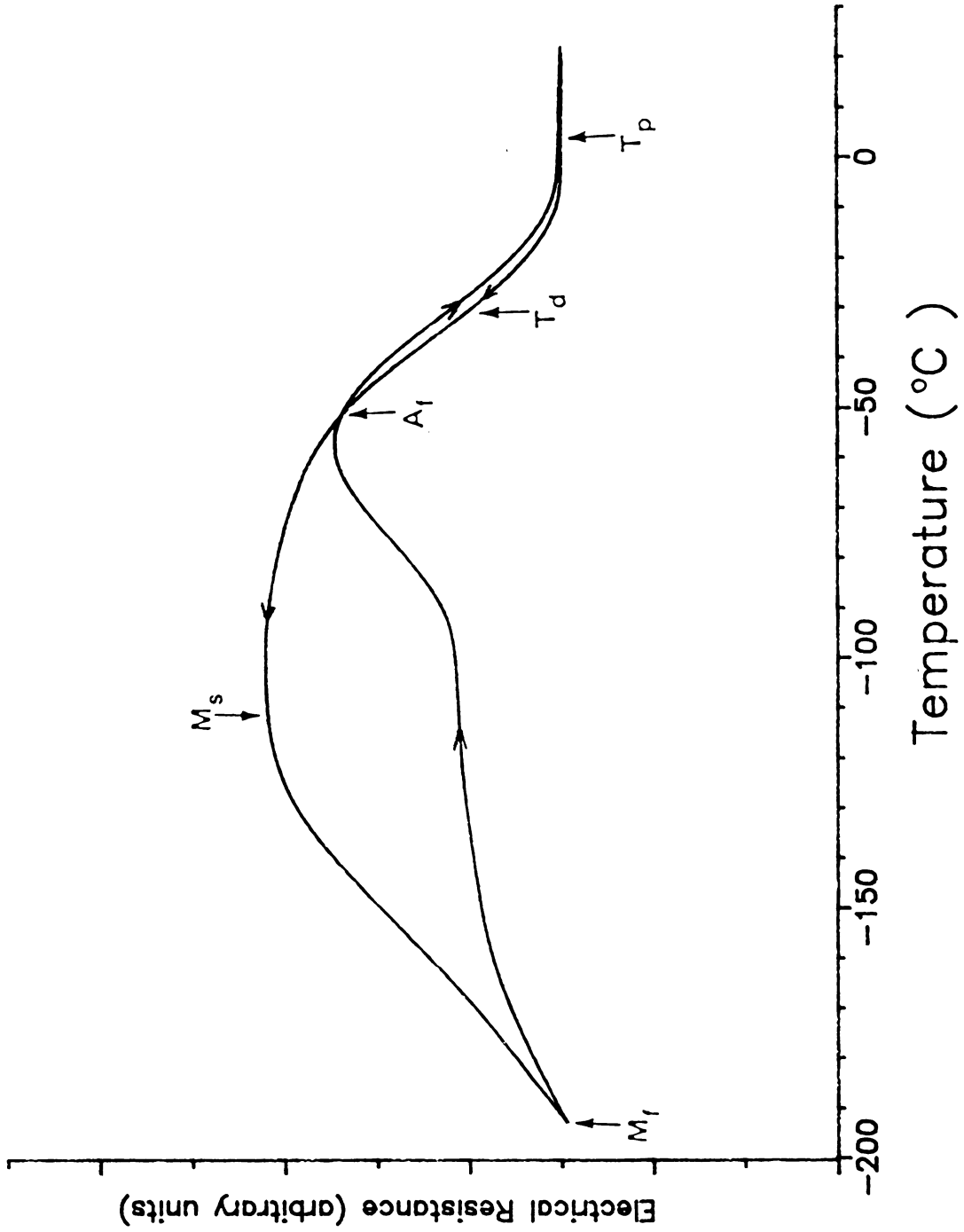


Fig 2. Electrical resistance vs. temperature curve for the 50th full thermal cycled specimen.



specimen are given in Table I.

Fig.3 shows a transmission electron micrograph and corresponding diffraction patterns of the parent phase of the $\text{Ti}_{495}\text{Ni}_{48}\text{Cr}_{25}$ alloy taken at room temperature. The Bright field image in Fig.3(a) shows a mottling, 'tweed-like' structure as reported earlier in TiNi alloys (25). In Fig.3(b), the diffraction pattern shows the weak $1/3$ superlattice reflections. By measuring the distance between the fundamental spots and the superlattice spots, it is found that the positions of the superlattice reflections are deviated slightly from the exact $1/3$ position. In addition to the weak $1/3$ superlattice reflections, the diffraction patterns in Fig.3(b) and (c) shows the diffuse streaks, arcs and interlocking rings.

These diffraction patterns seems to be quite similar to the diffraction patterns taken from the incommensurate phase in the $\text{Ti}_{587}\text{Ni}_{375}\text{Al}_{38}$ alloy. The diffraction patterns were explained as the intersections of the Ewald sphere with non-spherical, curved surfaces in the reciprocal space and possibly related to the Fermi surface geometry of this alloy (14).

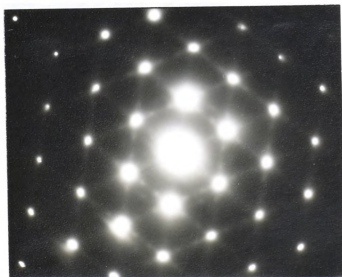
From the results obtained from the electrical resistance vs. temperature measurement, the T_p temperature of the bulk specimen is about 7°C , close to the room temperature. The transformation temperature of the thin foil could be slightly different from that of the bulk material. By considering the above facts, it might be thought that a

TABLE I. Transformation temperatures of the as-annealed and the thermal-cycled $\text{Ti}_{49.5}\text{Ni}_{48}\text{Cr}_{2.5}$ alloy.

(°C)	Ms	M_f	As	A_f	T_p	T_d
As-annealed	-108	<-196	-92	-49	7	-33
50th cycle	-110	<-196	-93	-51	5	-33

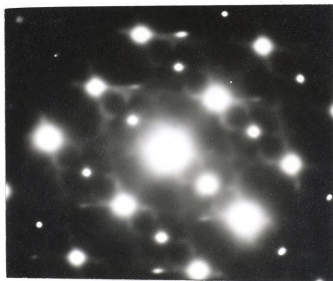


(a)



(b)

Fig.3 Transmission electron micrograph and corresponding diffraction patterns of the parent phase of the $Ti_{49.5}Ni_{48}Cr_{2.5}$ alloy taken at room temperature. (a) Bright field image (x50,000); (b) $[111]_{B2}$ zone diffraction pattern.



(c)

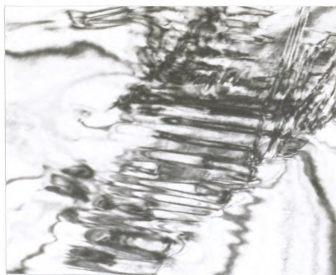
Fig.3 (Continued). (c) $[110]_{B_2}$ zone diffraction pattern.

thin foil is undergoing the very early stage of the parent-to-incommensurate transition.

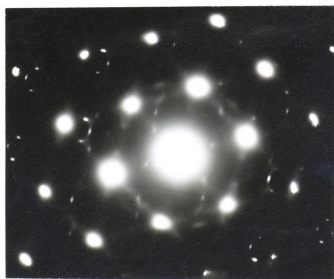
Fig.4 shows another transmission electron micrograph and the corresponding diffraction pattern taken at room temperature. In Fig.4(a), small 'needle-like' structures are shown. A corresponding diffraction pattern in Fig.4(b) shows that the intensity of some of inner $1/3$ (110) type reflections is increased and the additional superlattice reflections, which seems to be connected by small interlocking rings, appear. Fig.4(c) is a dark field image of Fig.4(a) taken by using three superlattice reflections forming a small interlocking ring. The dark field image shows one variant of needle-like structures. Thus, it can be considered that one variant of needle-like structures might create thoes interlockings.

The exact nature and the origin of these 'needle-like' structures is not clear at this moment. However, these are not the same as the 'needle' domains of the commensurate phase in TiNiFe and TiNiAl alloys, considering that the thin foil is in the very early stage of the parent-to-incommensurate phase transition.

Fig.5 shows a scanning transmission electron micrograph taken at -136°C and corresponding diffraction patterns of the $\text{Ti}_{49.5}\text{Ni}_{48}\text{Cr}_{25}$ alloy taken at -136°C and room temperature. In Fig5(a), Two variants of 'needle' domains of the commensurate phase are shown. Although the temperature is below the M_s temperature of a bulk material, no



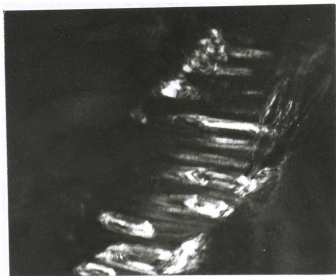
(a)



(b)

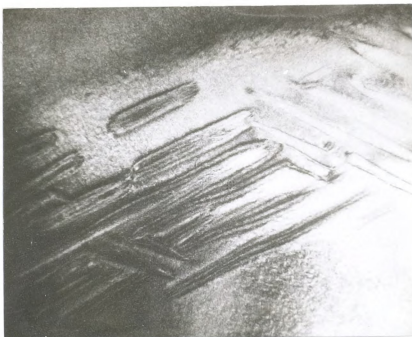
Fig.4 Transmission electron micrographs and corresponding diffraction pattern of the $\text{Ti}_{49.5}\text{Ni}_{48}\text{Cr}_{2.5}$ alloy taken at room temperature. (a) Bright field image (x40,000) (b) $[111]_{\text{B2}}$ zone diffraction pattern.



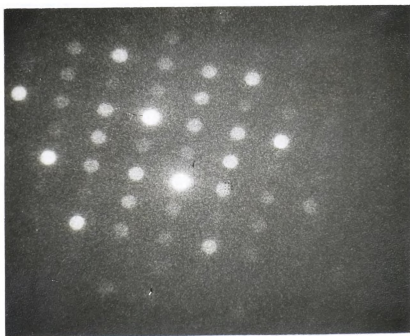


(c)

Fig.4 (Continued). (c) Dark field image (x40,000).

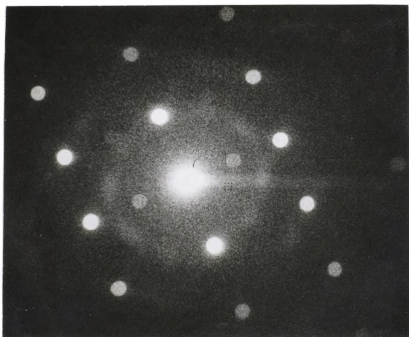


(a)



(b)

Fig.5 Scanning transmission electron micrograph taken at -136°C and corresponding diffraction patterns taken at -136°C and room temperature. (a) Bright field image ($\times 50,000$) ; (b) Selected area diffraction pattern taken at -136°C



(c)

Fig.5 (Continued). (c) $[110]_{B_2}$ zone diffraction pattern taken at room temperature.

martensite phase can be seen. It might be ascribed to the thin foil effect. It has been reported that the martensite plates begin to form at thicker regions of a thin foil.

A corresponding selected area diffraction pattern in Fig.5(b), taken from one of two variants, clearly shows the characteristic $1/3$ (111) type superlattice reflections at the exact $1/3$ positions. Fig.5(c) shows the diffuse $[110]_{B2}$ zone diffraction pattern taken at room temperature. No $1/3$ superlattice reflections can be seen. Thus, it is clear that $Ti_{49.5}Ni_{48}Cr_{25}$ alloy does undergo the second premartensitic transformation.

From the results obtained, it can be considered that $Ti_{49.5}Ni_{48}Cr_{25}$ alloy exhibits similar CDW transition phenomena observed in TiNiFe and TiNiAl alloys.

Aging effects

The effect of aging on the transformation temperatures of the $Ti_{49.5}Ni_{48}Cr_{25}$ alloy is given in Table II. Fig.6(a)-(f) shows the electrical resistance vs. temperature curves of $Ti_{49.5}Ni_{48}Cr_{25}$ alloy aged at $400^\circ C$ with varying the aging time from 5 min. to 24 hrs. In general, the M_s temperature of specimens aged at $400^\circ C$ continues to decrease with a longer aging time. It can also be seen that the shape of the curve is obviously changed and the decreasing rate of M_s temperature is increased after aging for 12 hrs. The difference of resistance between the cooling and heating curve becomes narrow after aging for 12 hrs. The electrical resistance of specimens around the M_f temperature is found

TABLE II. The effect of aging on the transformation temperatures of the $\text{Ti}_{49.5}\text{Ni}_{48}\text{Cr}_{2.5}$ alloy.

($^{\circ}\text{C}$)		M_s	M_f	A_s	A_f	T_p	T_d
400 $^{\circ}\text{C}$	5 min.	-118	<-196	-100	-59	2	-36
	30 min.	-117	<-196	-89	-57	0	-36
	1 hr.	-121	<-196	-97	-59	-7	-45
	4 hrs.	-123	<-196	-113	-70	-2	-45
	12 hrs.	-132	<-196		-78	-2	-46
	24 hrs.	-142	<-196		-79	-2	-48

500 $^{\circ}\text{C}$	5 min.	-108	<-196	-98	-55	7	-37
	30 min.	-109	<-196	-89	-49	6	-33
	1 hr.	-112	<-196	-97	-56	-1	-35
	4 hrs.	-135	<-196	-115	-75	-1	-46
	12 hrs.	-113	<-196	-103	-57	-1	-38
	24 hrs.	-100	<-196	-98	-45	7	-34

600 $^{\circ}\text{C}$	5 min.	-112	<-196	-104	-56	3	-37
	30 min.	-106	<-196	-89	-46	-3	-31
	1 hr.	-108	<-196	-93	-49	-3	-36
	4 hrs.	-113	<-196	-109	-57	-3	-37
	12 hrs.	-111	<-196	-100	-61	-3	-42
	24 hrs.	-90	-190	-94	-38	7	-30

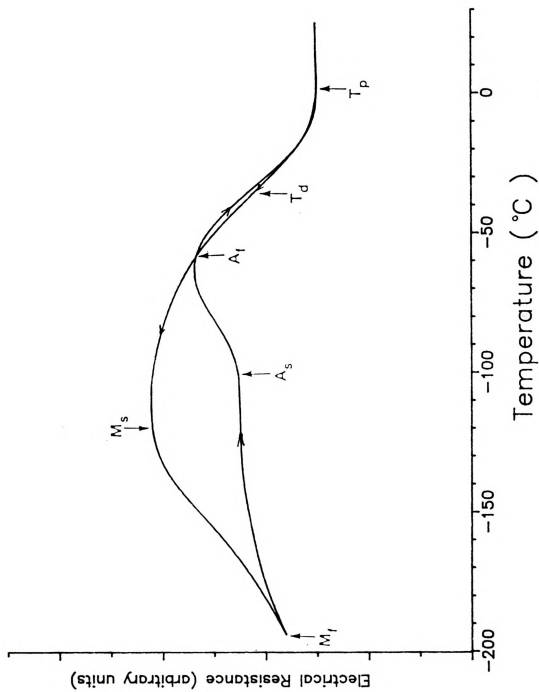


Fig. 6(a) Electrical resistance vs. temperature curve for the $Ti_{49.5}Ni_{48}Cr_{2.5}$ alloy aged at 400 °C for 5 min..

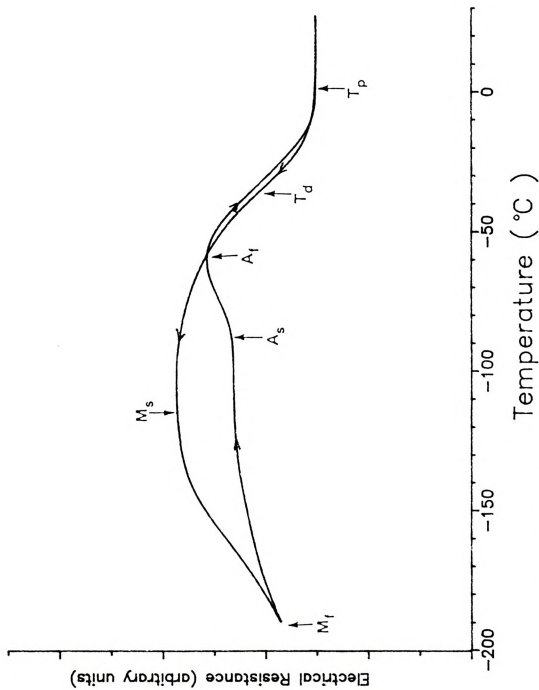


Fig. 6(b) Electrical resistance vs. temperature curve for the $Ti_{49.5}Ni_{48}Cr_{2.5}$ alloy aged at 400°C for 30 min..



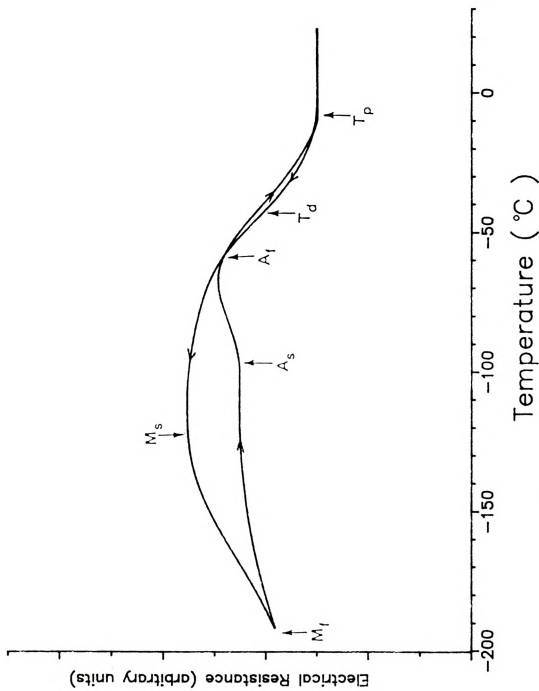


Fig. 6(c) Electrical resistance vs. temperature curve for the Ti_{49.5}Ni₄₈Cr_{2.5} alloy aged at 400°C for 1 hr..

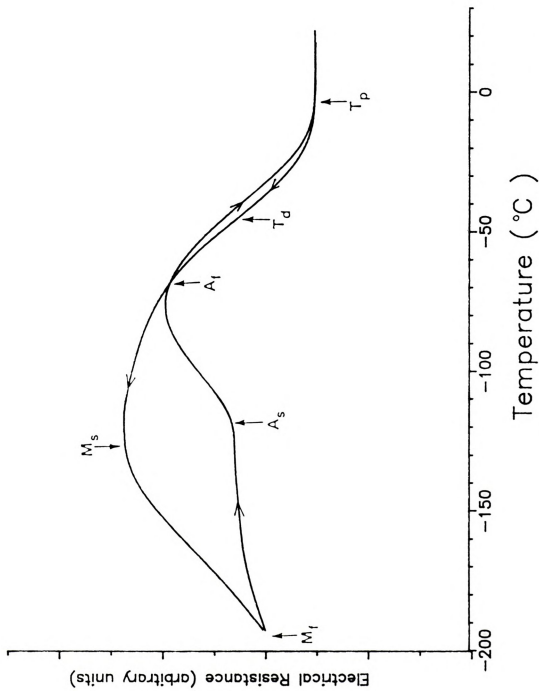


Fig. 6(d) Electrical resistance vs. temperature curve for the $Ti_{49.5}Ni_{48}Cr_{2.5}$ alloy aged at 400°C for 4 hrs..

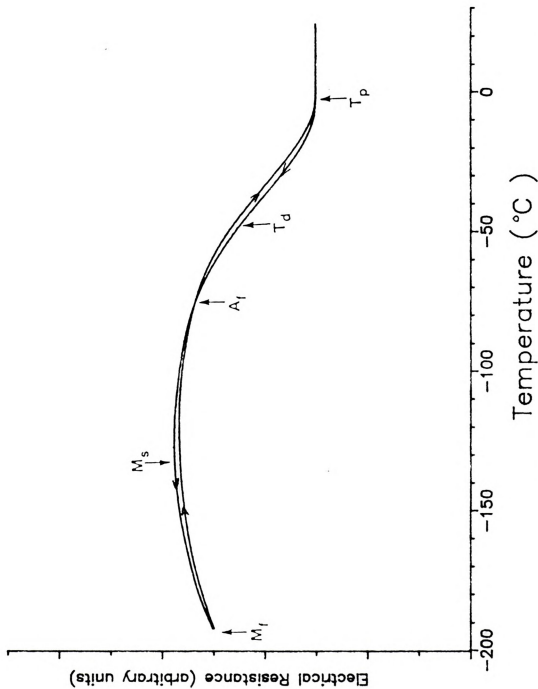


Fig. 6(e) Electrical resistance vs. temperature curve for the $\text{Ti}_{49.5}\text{Ni}_{48}\text{Cr}_{2.5}$ alloy aged at 400°C for 12 hrs..



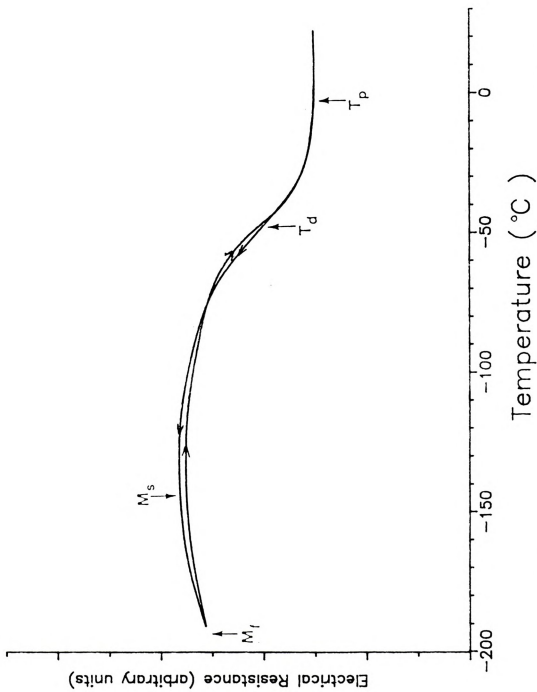


Fig. 6(f) Electrical resistance vs. temperature curve for the $\text{Ti}_{49.5}\text{Ni}_{48}\text{Cr}_{2.5}$ alloy aged at 400°C for 24 hrs..



to be increased with increasing aging time. It has been reported that the martensite phase decreases the electrical resistance in TiNi type alloys.

From the above results, it can be considered that the changes in the transformation temperatures and electrical resistance are due to the changes in the microstructure of the specimens, possibly the precipitates.

Fig.7 shows the transmission electron micrographs of the specimens aged at 400 °C for 1 hr, 4 hr. and 12 hrs. The extremely fine precipitates are shown and they appear to be coherent to the matrix. The size of the precipitates seems to be unchanged as the aging time increases.

According to the Ti-Ni phase diagram, TiNi phase in a Ti-rich alloy will decompose into 'Ti₂Ni' phase (26). The crystal structure of Ti₂Ni phase was reported to be fcc structure (27). Although the exact composition of the precipitates in Ti_{49.5}Ni₄₈Cr_{2.5} alloy is not known, it is suspected that the composition of the precipitates will be near 'Ti₂Ni'.

The decrease in Ms temperature due to the precipitates can be explained by the two factors, which was proposed by Horbogen (28). The first factor is the compositional dependence of the Ms temperature and the second factor is the strengthening mechanism.

It is well-known that Ms temperature of the TiNi alloy decreases with increasing nickel content from the stoichiometric composition (29). The Ti-rich precipitates in





(a)



(b)

Fig.7 Transmission electron micrographs of the $\text{Ti}_{49.5}\text{Ni}_{48}\text{Cr}_{2.5}$ alloy aged at $400\text{ }^\circ\text{C}$. (a) Bright field image (x60,000), aged for 1 hr. ; (b) Bright field image (x60,000), aged for 4hrs..



(c)

Fig.7 (Continued). (c) Bright field image (x60,000), aged for 12 hrs..



this alloy will increase the nickel content of the matrix phase, depressing the M_s temperature. The precipitates are extremely fine and coherent to the matrix. Thus, these precipitates can increase the strength of matrix phase and the initiation of the martensitic transformation will be more difficult.

The electrical resistance vs. temperature curves of the $Ti_{49.5}Ni_{48}Cr_{2.5}$ alloy aged at $500^\circ C$ are shown in Fig.8(a)-(f). It can be found that the electrical resistance is increasing up to the aging for 4 hrs, which corresponding to the minimum M_s temperature. Aging for a longer time after 4 hrs decreases the electrical resistance and increases the M_s temperature.

The variation of M_s temperature vs. aging time for specimens aged at $500^\circ C$ is quite different from that of specimens aged at $400^\circ C$, as can be seen in Fig.12(a). This can be explained as follows. The M_s temperature is almost unchanged up to the aging for 30 min. In case of 1 hr. aging treatment, M_s temperature is slightly decreased, which can be recognized as the onset of the precipitation. M_s temperature is further decreased up to aging for 4 hrs. and stops to decrease, corresponding to the finishing point of the precipitation. Aging for a longer time increases the M_s temperature. It might be the overaging effect due to the coarsening of the precipitates. The mechanism of the M_s drops due to the precipitates is the same as in case of $400^\circ C$ aging treatment. In addition, the coarse precipitates

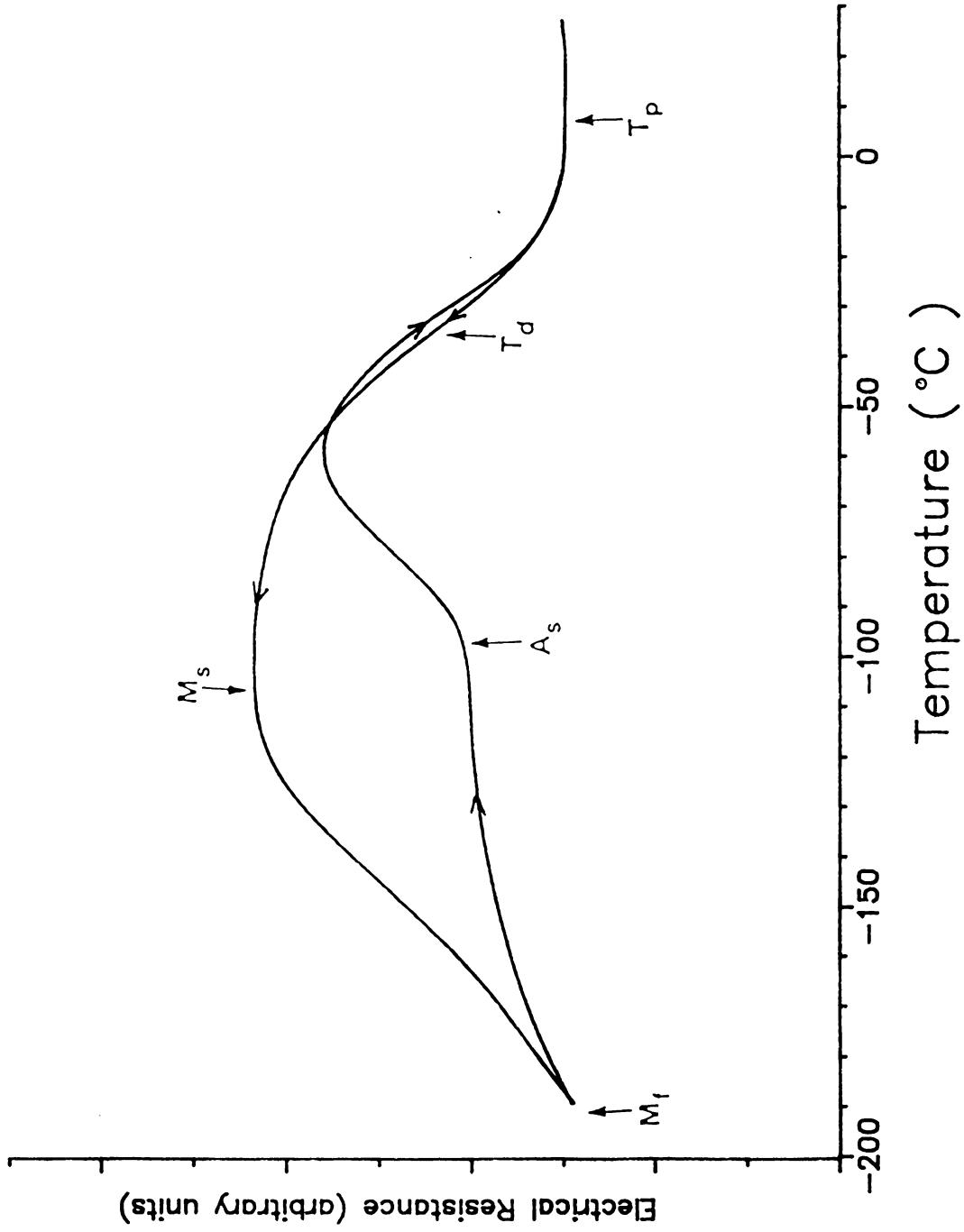


Fig.8(a) Electrical resistance vs. temperature curve for the $\text{Ti}_{49.5}\text{Ni}_{48}\text{Cr}_{2.5}$ alloy aged at 500°C for 5 min..



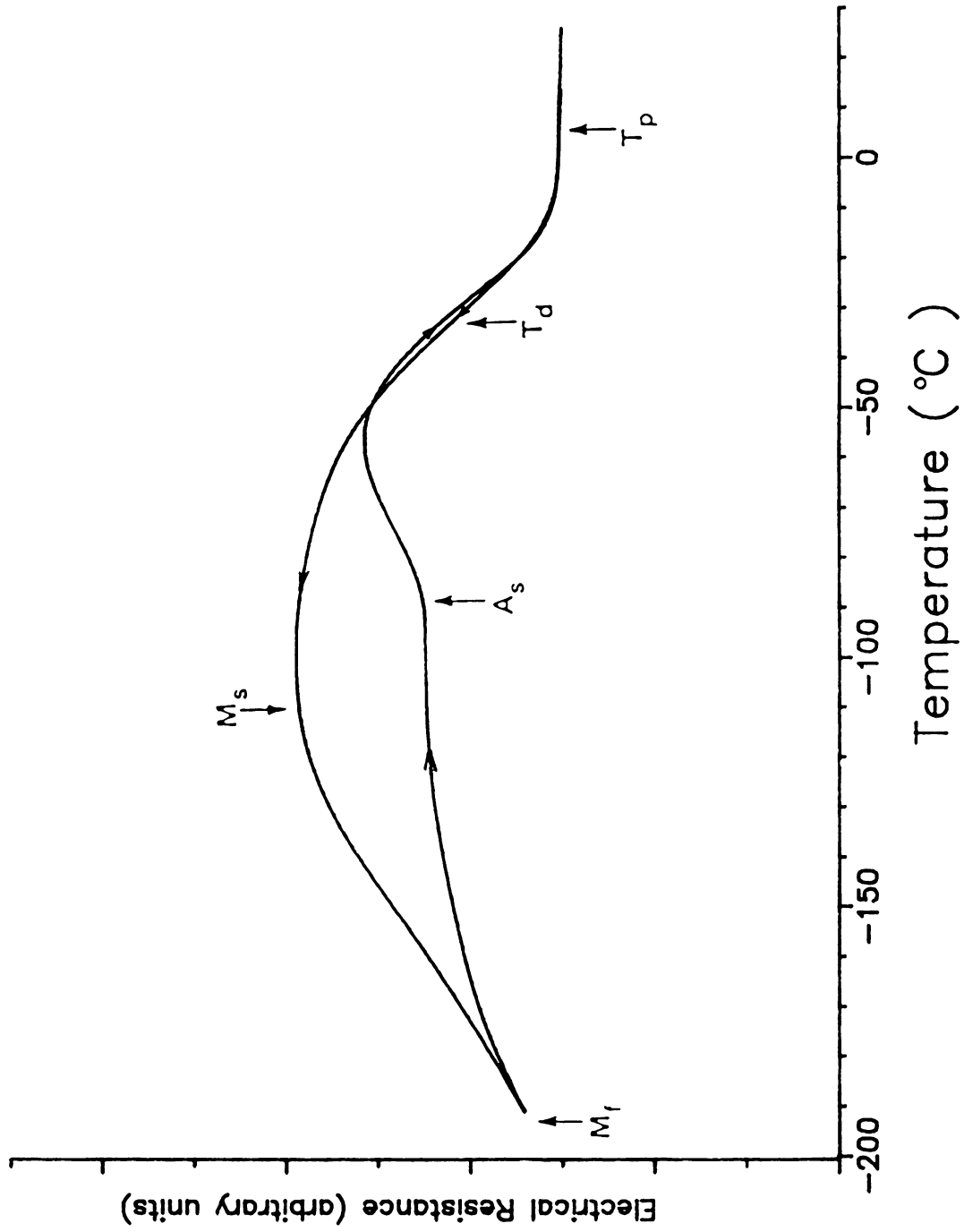


Fig. 8(b) Electrical resistance vs. temperature curve for the Ti_{49.5}Ni₄₈Cr_{2.5} alloy aged at 500 °C for 30 min..



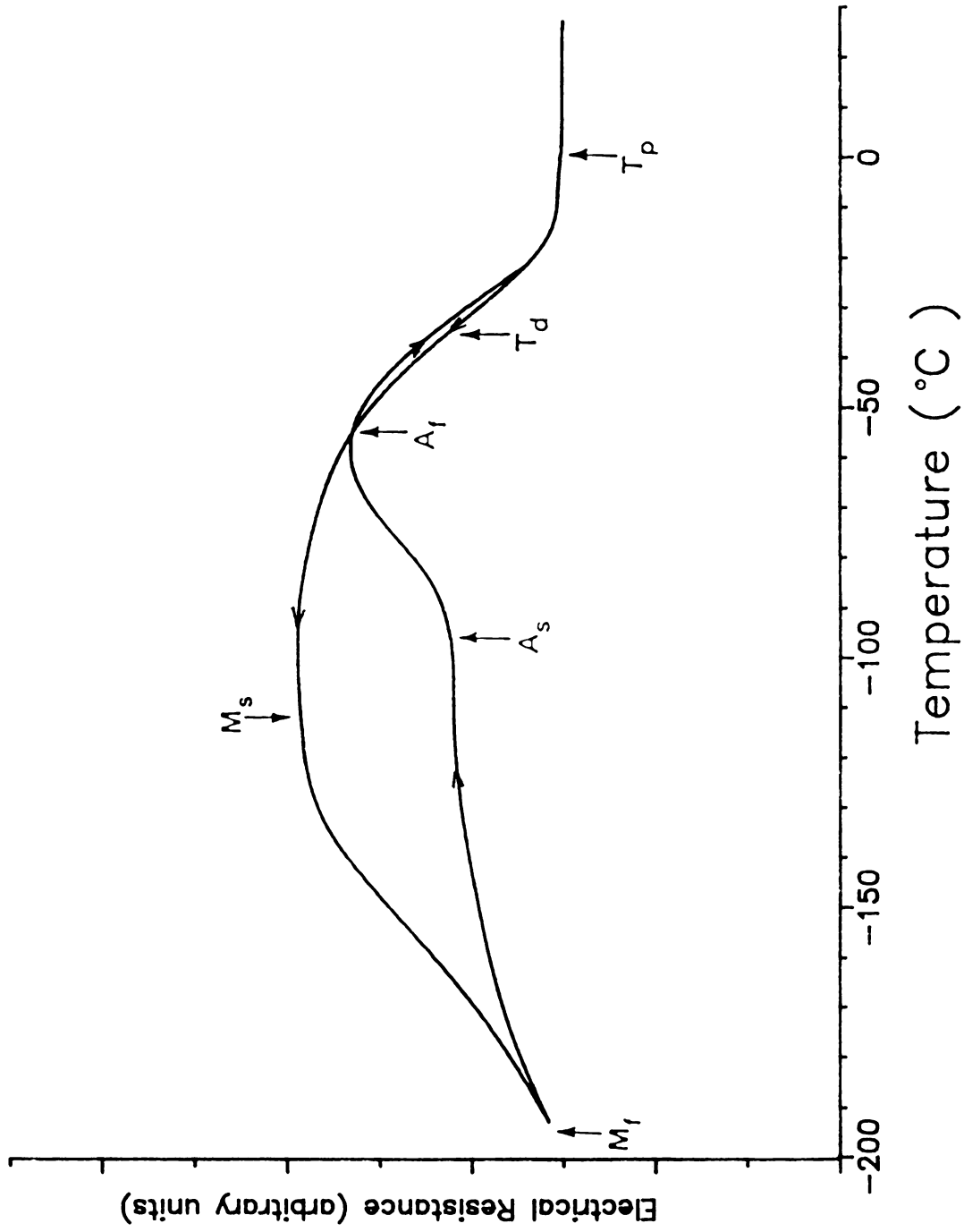


Fig. 8(c) Electrical resistance vs. temperature curve for the Ti_{49.5}Ni₄₈Cr_{2.5} alloy aged at 500°C for 1hr..



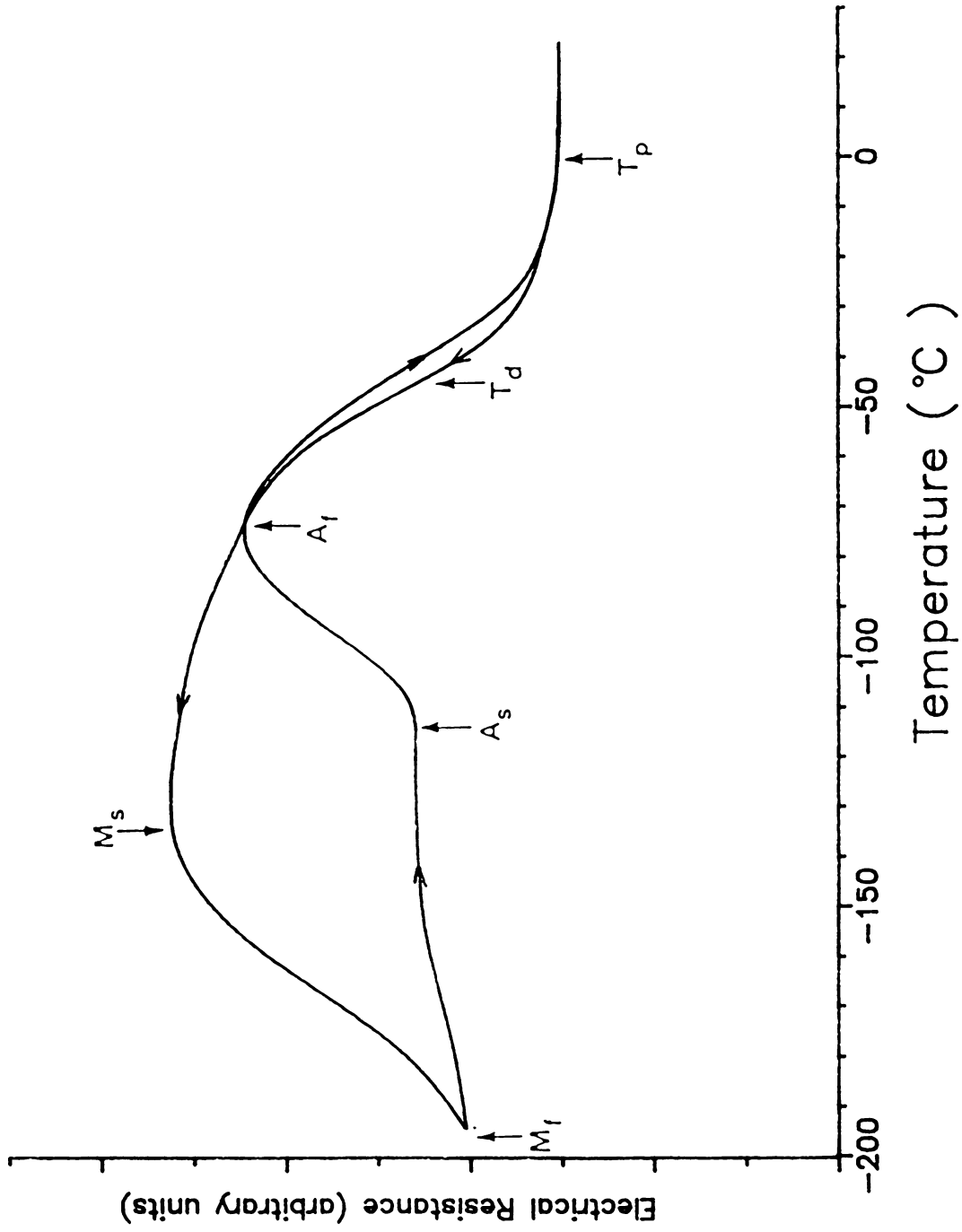


Fig.8(d) Electrical resistance vs. temperature curve for the Ti_{49.5}Ni₄₈Cr_{2.5} alloy aged at 500°C for 4 hrs..

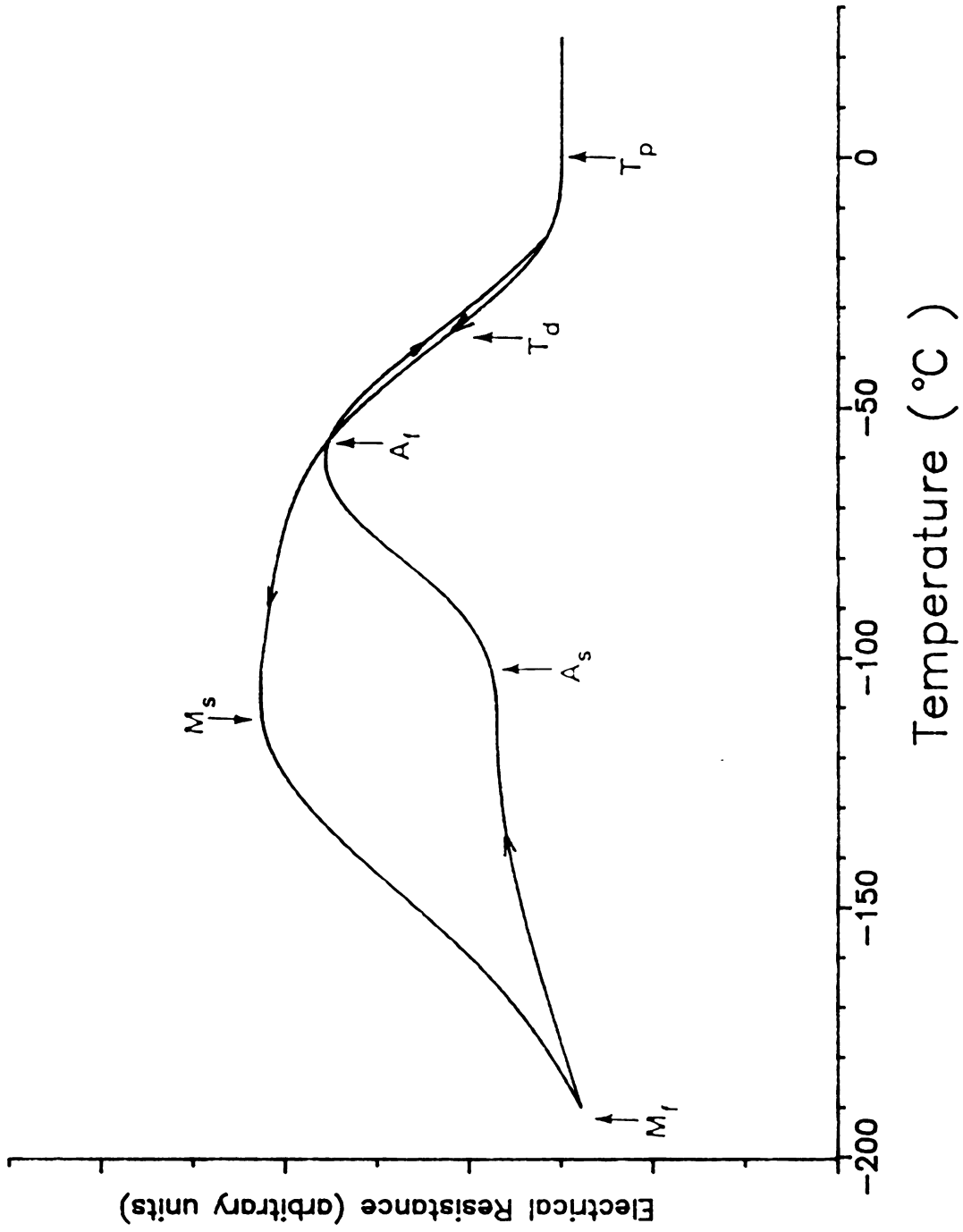


Fig.8(e) Electrical resistance vs. temperature curve for the Ti_{49.5}Ni₄₈Cr_{2.5} alloy aged at 500°C for 12 hrs..



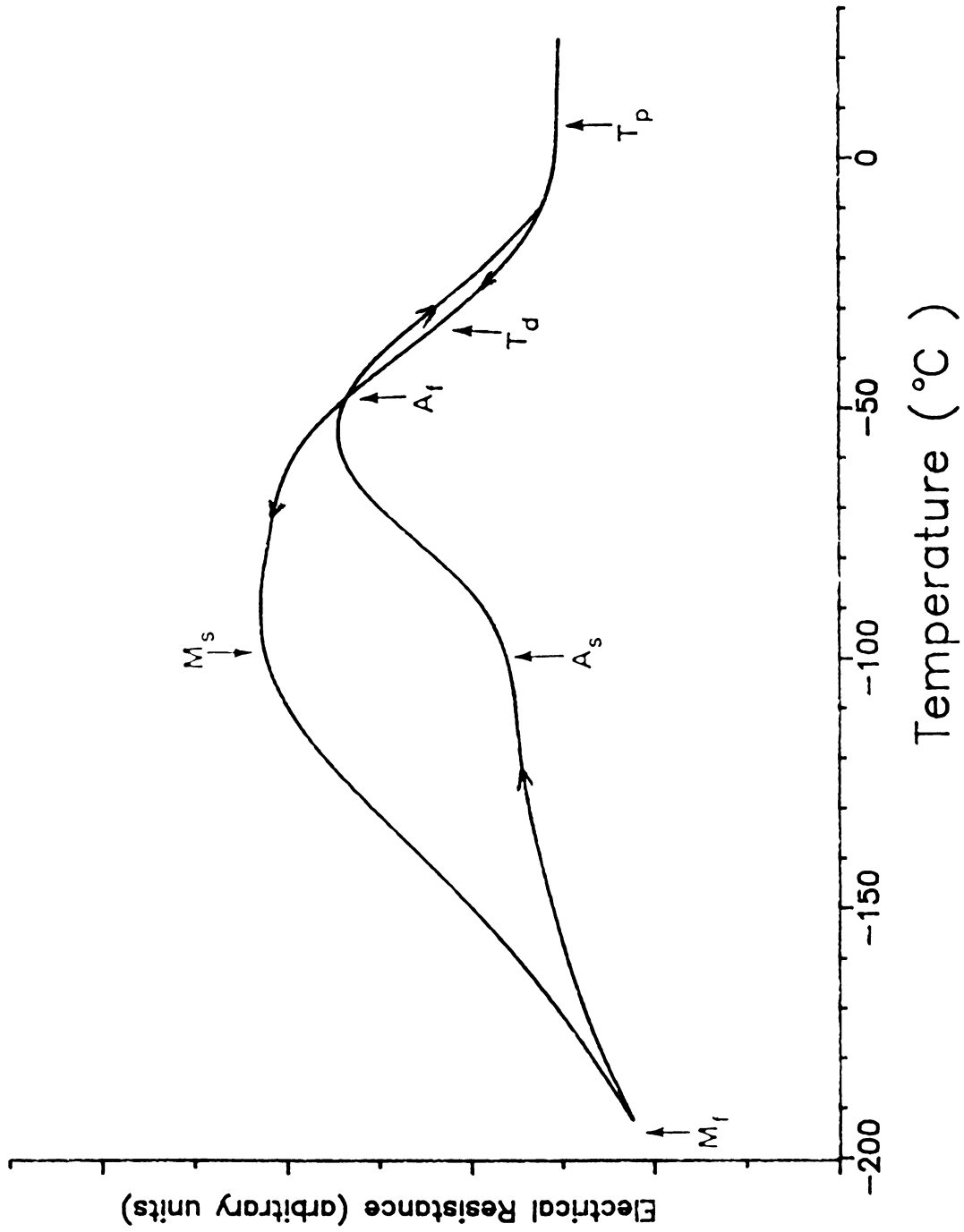


Fig. 8(f) Electrical resistance vs. temperature curve for the Ti_{49.5}Ni₄₈Cr_{2.5} alloy aged at 500 °C for 24 hrs..

might decrease the strength of the parent phase and , as a result, Ms temperature can be increased for specimens aged for a longer time.

Fig.9 shows the transmission electron micrographs of specimens aged at 500 °C for 1 hr., 4 hrs. and 12 hrs. Comparing the Fig.9(c) and 9(b), it is clear that the size of the precipitates in Fig.9(c) is larger than that of the precipitates in Fig.9(b).

The electrical resistance vs. temperature curves of the $Ti_{49.5}Ni_{48}Cr_{2.5}$ alloy aged at 600 °C are in Fig.10(a)-(f). In case of the 600 °C aging treatment, the general shape of curves is not changed greatly as in the case of the 500 °C aging treatment. In general, the effect of aging at 600 °C is not as obvious as that of aging at 500 °C. The electrical resistance increases for specimens aged for 4 hrs and 12 hrs, corresponding to a low Ms temperature. The electrical resistance of a specimen aged for 24 hrs. is markedly decreased and Ms temperature of this specimen is high as can be expected.

Fig.11 shows the transmission electron micrographs and selected area diffraction pattern of specimens aged at 600 °C. From Fig.11(a) to Fig.11(c), it can be seen that the precipitates are coarsening to a larger size. In Fig.11(c), the coherent strain contrasts around the precipitates are shown. The corresponding diffraction pattern in Fig.11(d) exhibits relatively strong streaks at the diffracted reflections. Fig11(e) is the dark field image taken by

1010

1011

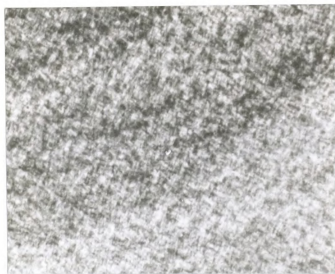
1012

1013

1014

1015

1



(a)



(b)

Fig.9 Transmission electron micrographs of the $\text{Ti}_{49.5}\text{Ni}_{48}\text{Cr}_{2.5}$ alloy aged at 500 °C. (a) Bright field image (x150,000), aged for 1 hr. ; (b) Bright field image (x150,000), aged for 4 hrs..



(c)

Fig.9 (Continued). (c) Bright field image (x150,000), aged for 12 hrs..

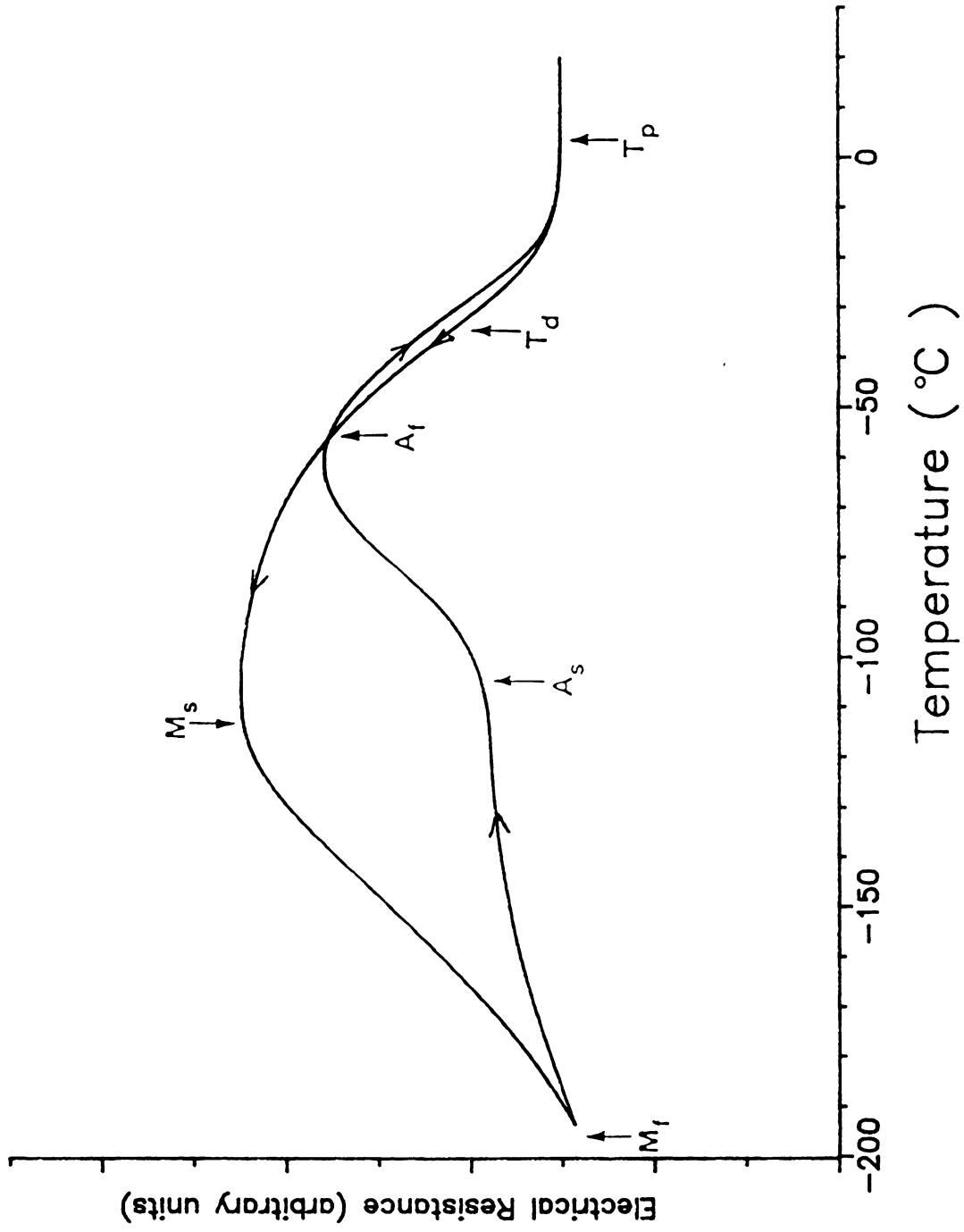
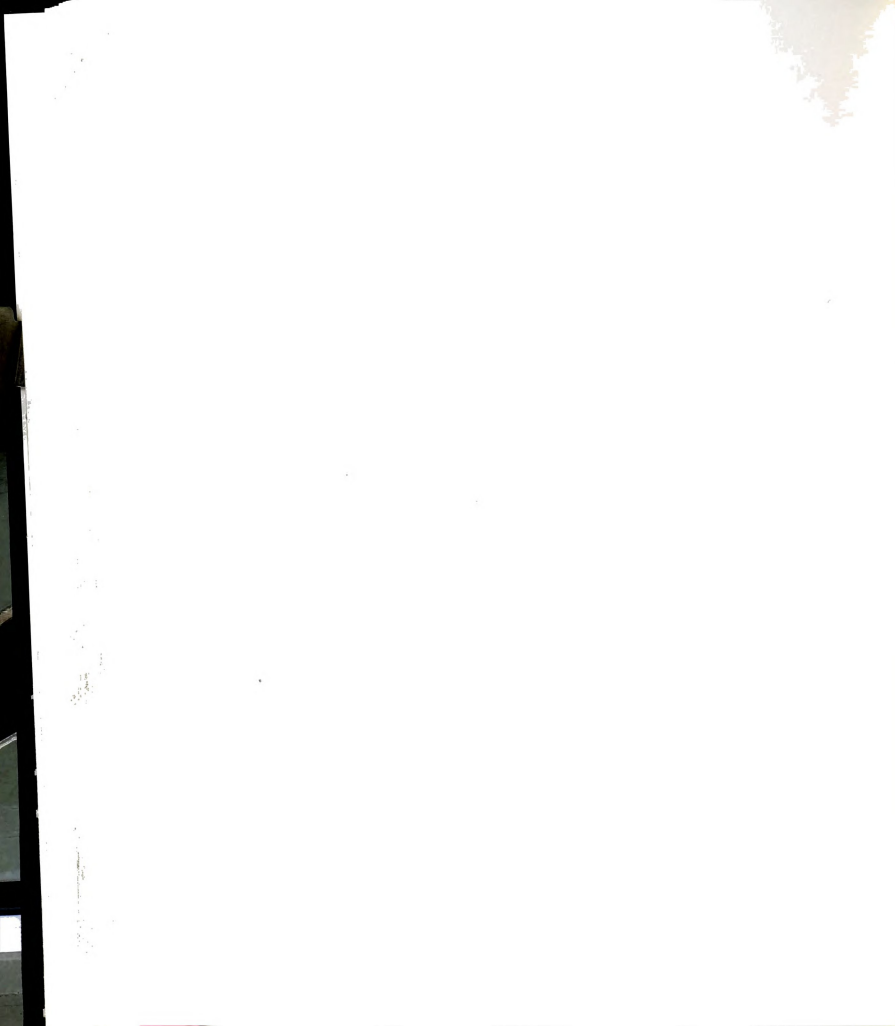


Fig.10(a) Electrical resistance vs. temperature curve for the $Ti_{49.5}Ni_{48}Cr_{2.5}$ alloy aged at $600^\circ C$ for 5 min..



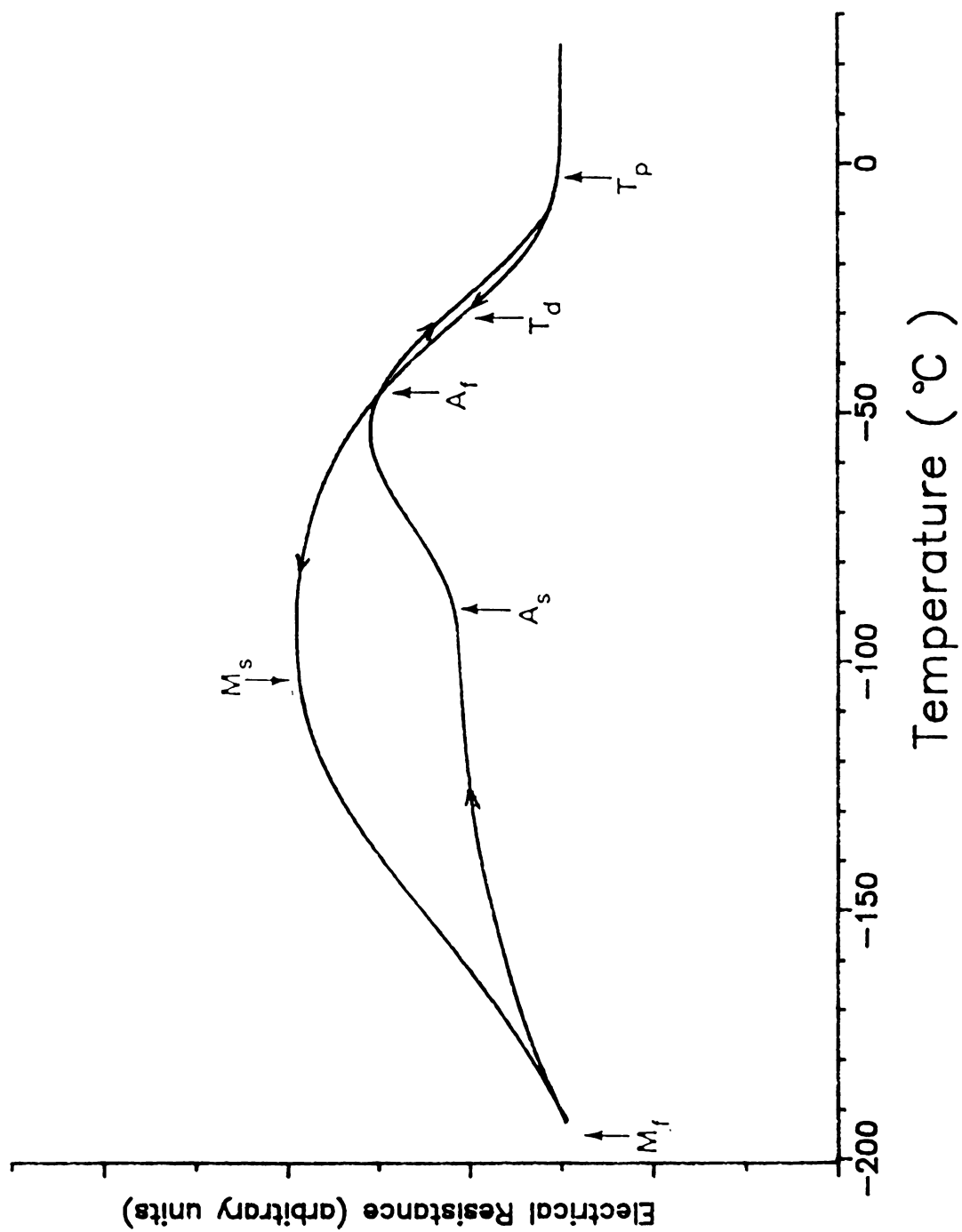


Fig.10(b) Electrical resistance vs. temperature curve for the $\text{Ti}_{49.5}\text{Ni}_{48}\text{Cr}_{2.5}$ alloy aged at 600°C for 30 min..



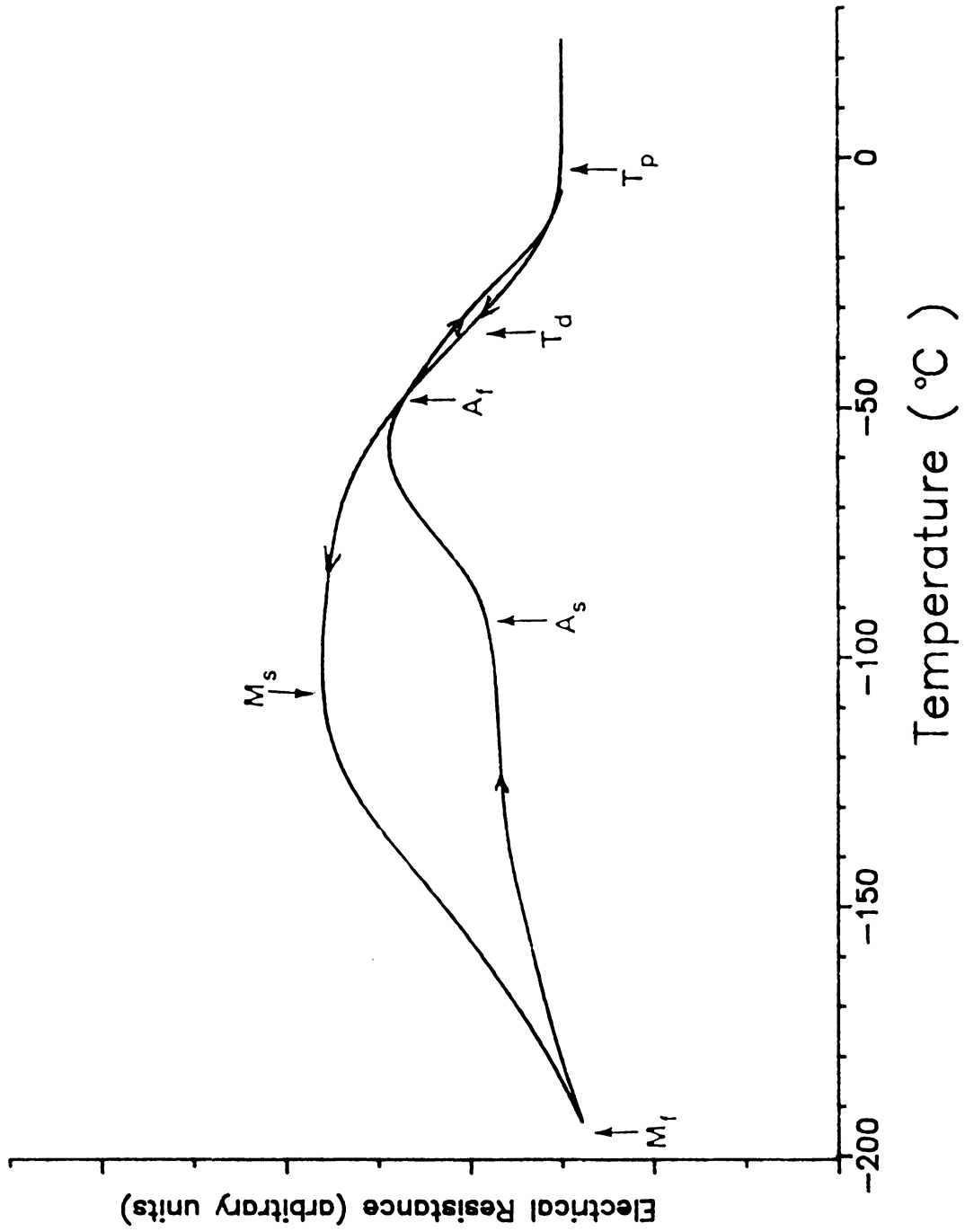


Fig.10(c) Electrical resistance vs. temperature curve for the Ti_{49.5}Ni₄₈Cr_{2.5} alloy aged at 600°C for 1hr..



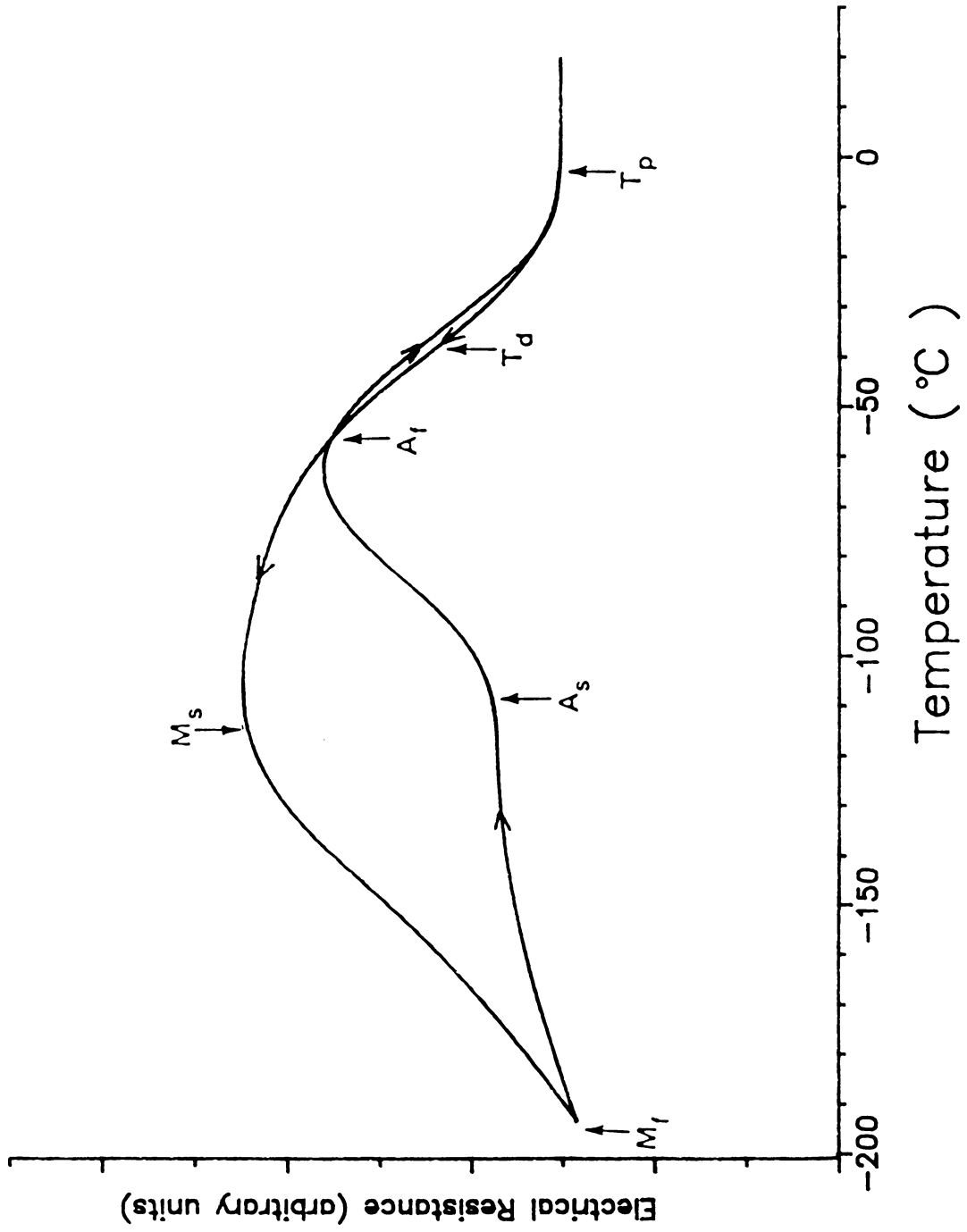


Fig.10(d) Electrical resistance vs. temperature curve for the $Ti_{49.5}Ni_{48}Cr_{2.5}$ alloy aged at $600^\circ C$ for 4 hrs...

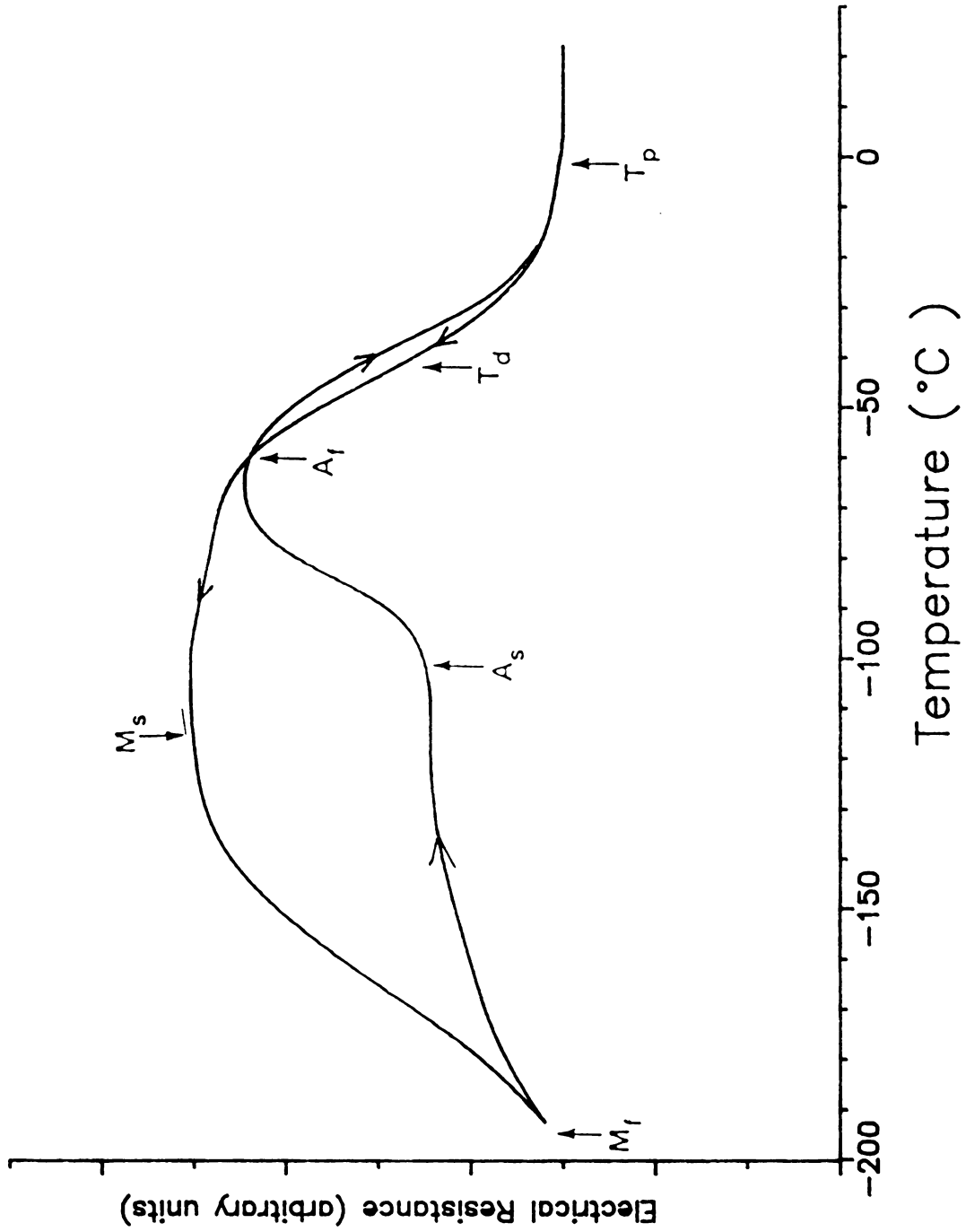


Fig.10(e) Electrical resistance vs. temperature curve for the $\text{Ti}_{49.5}\text{Ni}_{48}\text{Cr}_{2.5}$ alloy aged at 600°C for 12 hrs..



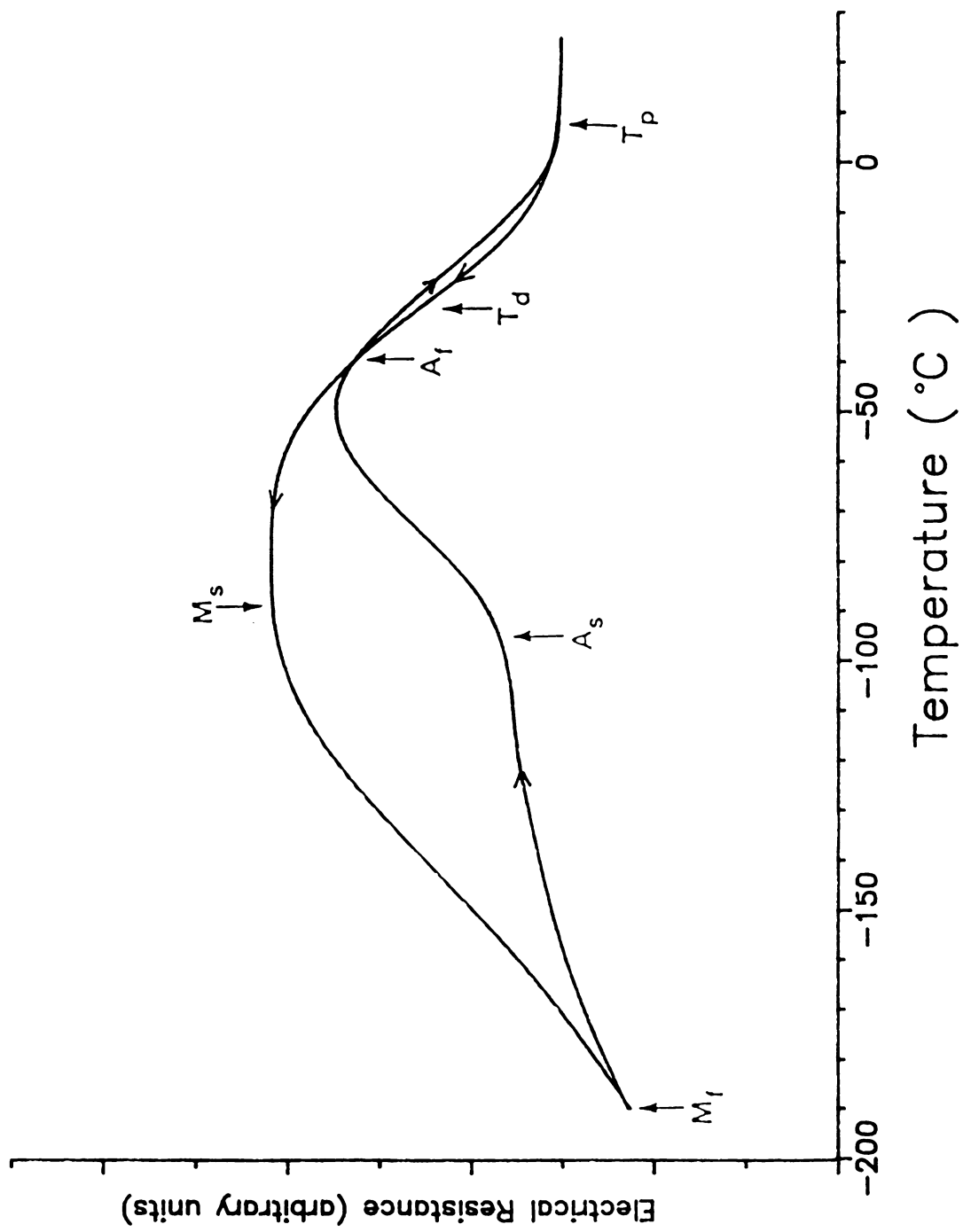


Fig.10(f) Electrical resistance vs. temperature curve for the $Ti_{49.5}Ni_{48}Cr_{2.5}$ alloy aged at $600^{\circ}C$ for 24 hrs..



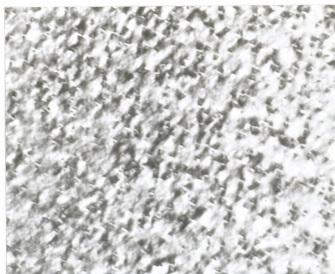


(a)

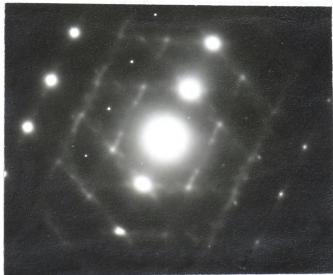


(b)

Fig.11 Transmission electron micrographs and selected area diffraction pattern of the $\text{Ti}_{49.5}\text{Ni}_{48}\text{Cr}_{2.5}$ alloy aged at 600°C . (a) Bright field image ($\times 150,000$), aged for 1 hr. ; (b) Bright field image ($\times 150,000$), aged for 4 hrs..

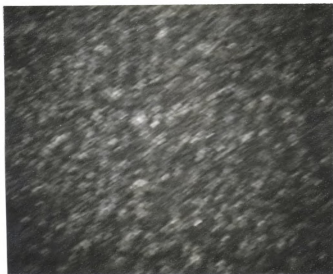


(c)



(d)

Fig.11 (Continued). (c) Bright field image (x150,000), aged for 24 hrs. ; (d) $[211]_{B_2}$ zone diffraction pattern.



(e)

Fig.11 (Continued). (e) Dark field image ($\times 150,000$), aged for 24 hrs..



including the diffracted reflections and streaks. Thus, the precipitates as well as the matrix phase are in contrast.

Fig.12(a)-(e) shows the variation of the transformation temperatures (M_s , A_s , A_f , T_p and T_d) vs. aging time at various temperatures. It can be seen that the variation of M_s , A_s and A_f temperature is quite similar each other. The variation of M_s temperature is mentioned earlier. Thus, the variation mode of A_s and A_f temperature can be explained. It is noticed that T_p and T_d are not significantly changed by the aging treatments.

Considering the fact that T_p and T_d are associated with the CDW transition and the CDW transition is electronic in origin, the effect of aging on these temperatures is expected to be small. The variation of T_d is larger than that of T_p . This might be ascribed to the difference in the order of transformation, that is, T_d represents the first order transformation temperature, whereas T_p represents the second order transition temperature.

Due to the lack of the additional diffraction spots from the precipitates, the crystal structure of this precipitate can not be obtained. By considering the fact that the streaks can be originated from the precipitates, the morphology of this precipitate is assumed to be the disc-shape. Further studies of larger precipitates by using X-rays, EDX and transmission electron microscopy will be necessary to obtain the exact crystal structure, composition and morphology of the precipitates in this alloy.



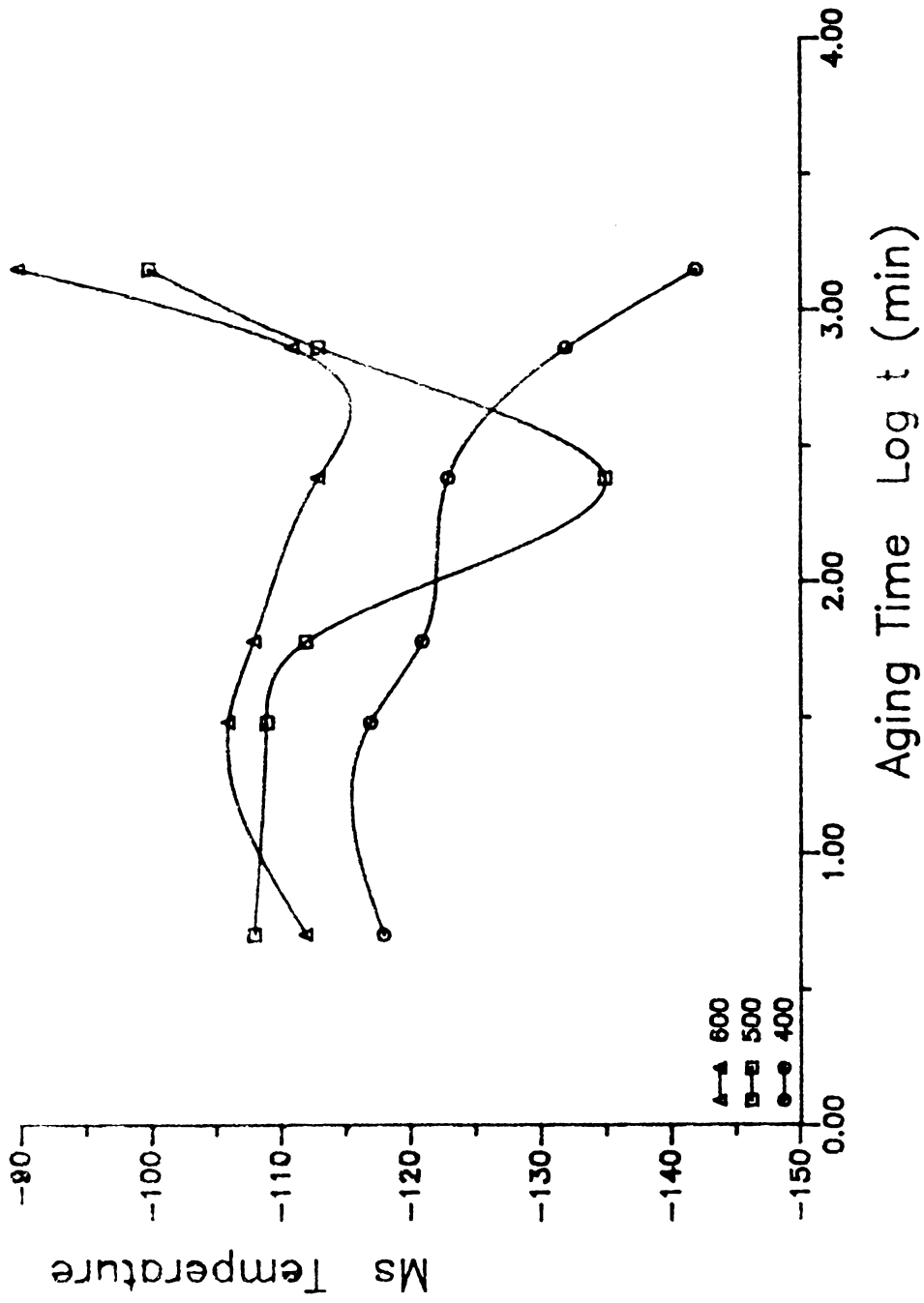


Fig.12(a) Variation of Ms Temperature vs. Aging Time



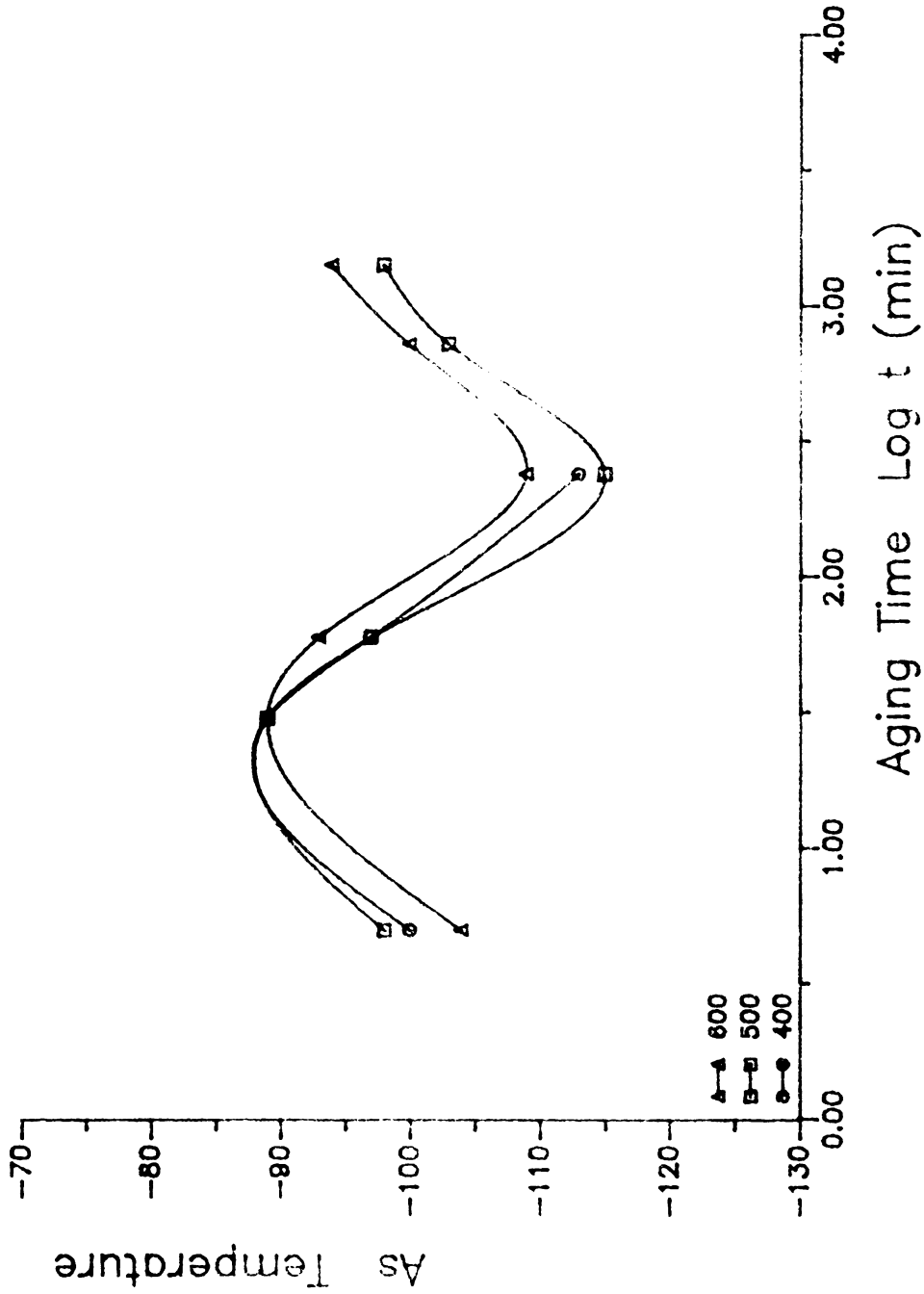


Fig.1 2(b) Variation of As Temperature vs. Aging Time



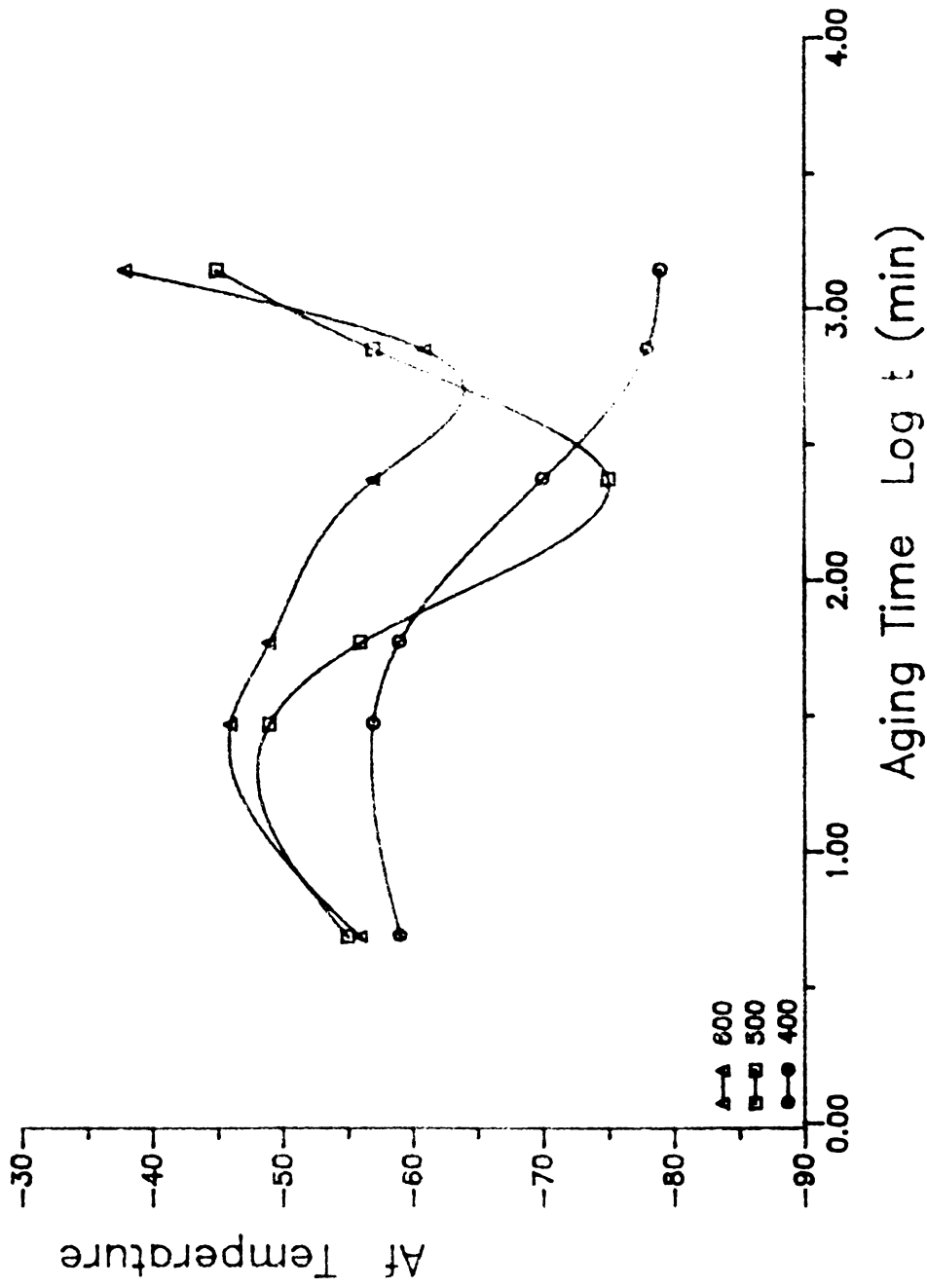


Fig.12(C) Variation of Af Temperature vs. Aging Time



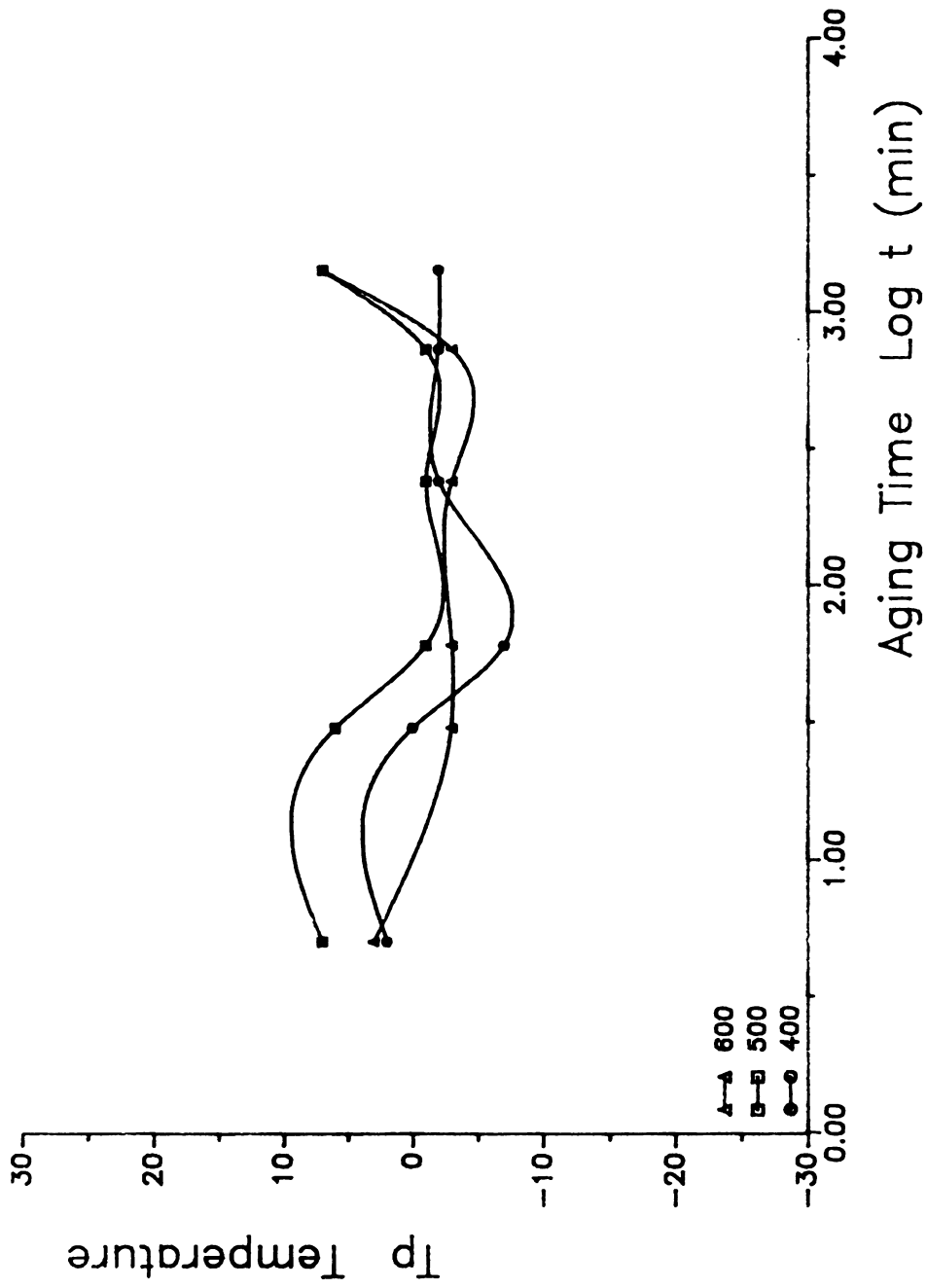


Fig.12(d) Variation of Tp Temperature vs. Aging Time



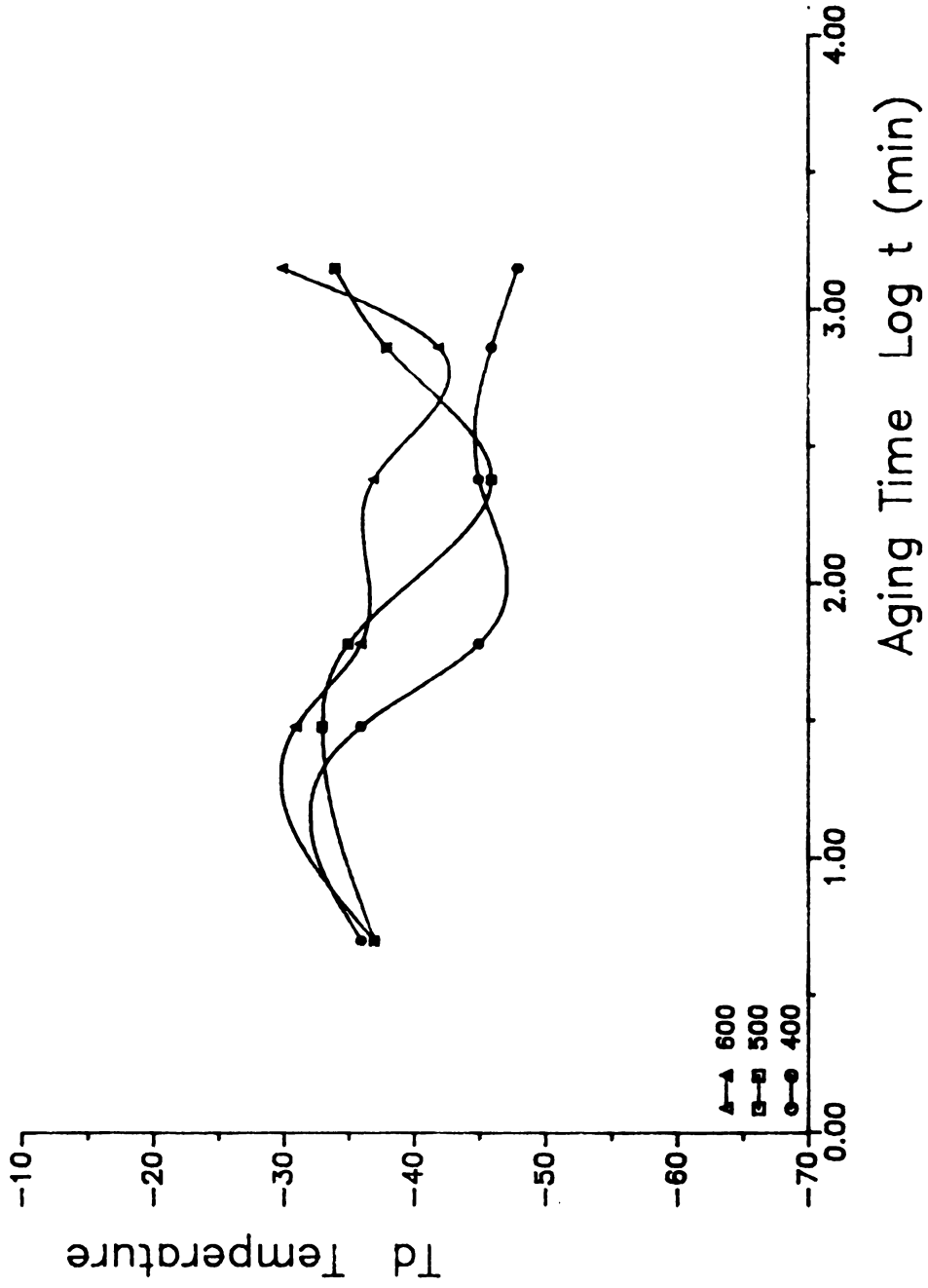


Fig.12(e) Variation of Td Temperature vs. Aging Time



Cold-rolling and cold-rolling plus aging effect

The electrical resistance vs. temperature curves of specimens, which were 20% cold-rolled and 20% cold-rolled followed by aging at 500 °C for 4 hrs., are given in Fig.13 and Fig.14, respectively. Table III shows the transformation temperatures of these specimens. The electrical resistance of the cold-rolled specimen is markedly decreased and, as a result, the shape of the curve is also changed greatly when comparing with that of the as-annealed one. The transformation temperatures except T_d are increased and especially, A temperature is markedly increased by 20% cold-rolling.

The transmission electron micrographs and corresponding diffraction patterns of a 20% cold-rolled specimen are shown in Fig.15. In Fig.15(a), a bright field image clearly shows two variants of the stress-induced martensite plates and the high density of dislocations. No particular internal structures of martensite are found in these stress-induced martensite plates.

A selected area diffraction pattern in Fig.15(b) is obtained from the parent phase area without a martensite plate. On the other hand, the selected area diffraction pattern in Fig.15(c) is obtained from the area including the martensite plates and the parent phase. The extra spots, which come from the stress-induced martensite plates, can be seen. This diffraction pattern is indexed by comparing the results of monoclinic ($B19'$) martensite in TiNi alloy,



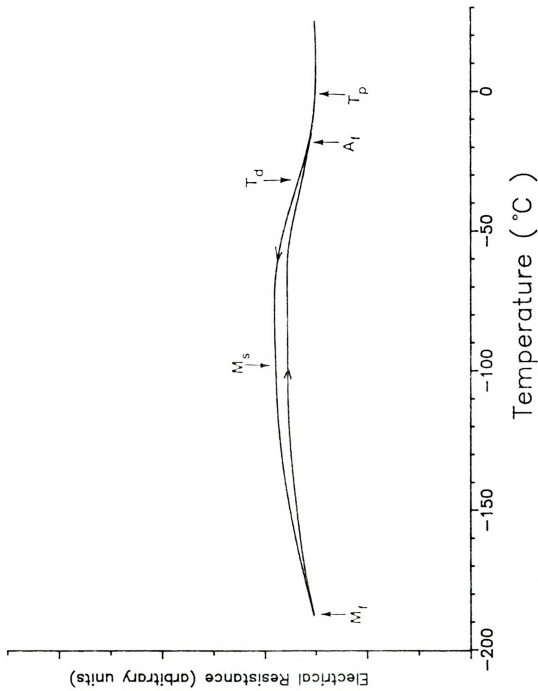


Fig.13 Electrical resistance vs. temperature curve for the Ti_{49.5}Ni₄₈Cr_{2.5} alloy, 20% cold-rolled.



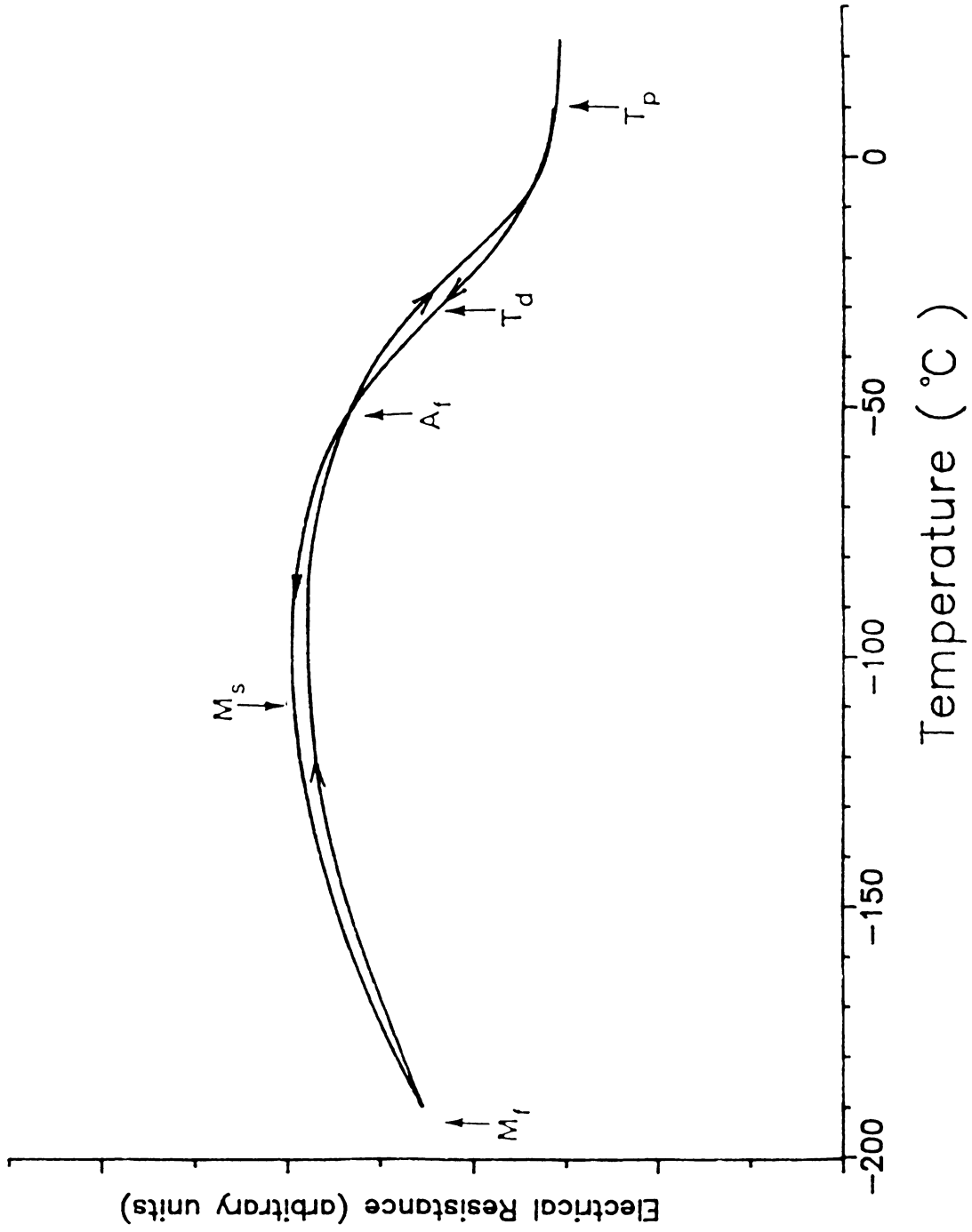


Fig.14 Electrical resistance vs. temperature curve for the $Ti_{49.5}Ni_{48}Cr_{2.5}$ alloy, 20% cold-rolled followed by aging at 500 °C for 4 hrs...



TABLE III. Transformation temperatures of the $\text{Ti}_{49.5}\text{Ni}_{48}\text{Cr}_{2.5}$ alloy, cold-rolled and cold-rolled followed by aging.

(°C)	Ms	M _f	As	A _f	T _p	T _d
20% cold-rolled	-97	-187	-	-19	-2	-13
20% cold-rolled + Aging at 500 °C for 4 hrs.	-109	<-196	-	-52	10	-32



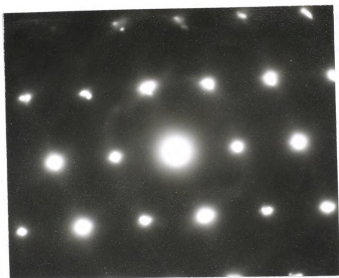


(a)

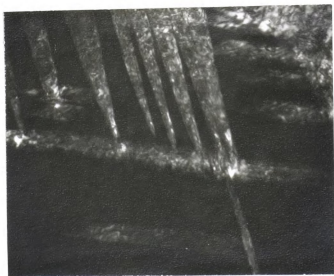


(b)

Fig.15 Transmission electron micrographs and corresponding diffraction patterns of $\text{Ti}_{49.5}\text{Ni}_{48}\text{Cr}_{2.5}$ alloy, 20% cold-rolled. (a) Bright field image (x50,000) ; (b) $[122]_{\text{B}_2}$ zone diffraction pattern.



(c)



(d)

Fig.15 (Continued). (c) $[122]_{B2}$ and $[\bar{1}\bar{1}\bar{1}]_{B19}$ zone diffraction pattern ; (d) Dark field image ($\times 60,000$).

which were reported earlier (6). The corresponding dark field image is obtained by using one of the reflections from the martensite plates and two variants of the stress-induced martensite plates are clearly shown.

From the above results, it can be considered that the decrease in the electrical resistance is due to the formation of stress-induced martensite plates. The increase in M_s temperature by cold-rolling might be analyzed as follows. The driving force necessary for transformation is reduced by a portion of the mechanical work performed by cold-rolling, and the stress-induced martensite plate produces stress fields in the surrounding parent phase and this can enhance the formation of the martensite by the autocatalytic effect.

The dislocations produced by cold-rolling and the interface between the parent and stress-induced martensite plates can provide the favorable nucleation sites for the martensitic transformation. The marked increase of the A_f temperature can be attributed to the stress-induced martensite plates, which can impede the reverse martensite-to-parent phase transformation.

The exact effects of cold-rolling on T_p and T_d are not fully understood. However, the decrease in T_p might be due to the changes in the geometry of Fermi-surface. If the deformation of the parent phase by cold-rolling can introduce the changes in the reciprocal lattice, the geometry of the Fermi-surface will change. This, in turn,

will change the premartensitic transition behaviour and temperatures.

By aging at 500 °C for 4 hrs, the electrical resistance of a 20% cold-rolled specimen rises as can be seen in Fig.14. This might be attributed to the disappearance of the stress-induced martensite plates. The values of the transformation temperatures are almost the same as that of the as-annealed one (Table III). Thus, it might be assumed that the effect of 20% cold-rolling is compensated by the effect of aging at 500 °C for 4 hrs.

Fig.16 shows the transformation electron micrographs of a cold-rolled and aged specimen. It can be seen that the stress-induced martensite plates are almost disappeared with leaving the dislocation arrays at the interfaces. The precipitates can also be observed in Fig.16(b).

100
100

100

100

100

100

100



(a)



(b)

Fig.16 Transmission electron micrographs of the $\text{Ti}_{49.5}\text{Ni}_{48}\text{Cr}_{2.5}$ alloy, 20% cold-rolled followed by aging at 500°C for 4 hrs. (a) Bright field image (x20,000) ; (b) Bright field image (x60,000).

IV. Summary

The electrical resistance vs. temperature measurements, and the electron diffraction and micrograph study show that the $\text{Ti}_{49.5}\text{Ni}_{48}\text{Cr}_{25}$ alloy exhibits the CDW transition phenomena, which was observed earlier in TiNiFe and TiNiAl alloys.

In general, the effect of aging on M_s , A_s and A_f temperature is more prominent than that of T_p and T_d . The aging effects are due to the Ti-rich precipitates. In the case of aging at 400°C , the M_s temperature continues to decrease up to an aging time of 24 hrs.

The variation of M_s temperature vs. aging time for specimens aged at 500°C shows a characteristic aging process including the starting and finishing of the precipitation. The effect of aging at 600°C is not as obvious as that of aging at 500°C .

The cycling effect on the transformation temperatures is not important in a $\text{Ti}_{49.5}\text{Ni}_{48}\text{Cr}_{25}$ alloy. Twenty percents cold-rolling treatment increases M_s temperature and decreases the electrical resistance of this alloy. These effects are due to the formation of stress-induced martensite plates. Aging at 500°C for 4 hrs after 20% cold-rolling changes the transformation temperatures of a cold-rolled specimen to the values of as-annealed one.



LIST OF REFERENCES

1. C.M. Wayman and K. Shimizu, *Met. Sci. J.*, 6 , 175 (1972)
2. D.P. Dautovich and G.R. Purdy, *Can. Metall. Q.*, 4 , 129 (1965)
3. H.C.Ling and R. Kaplow, *Met. Trans. A*, 11A , 77 (1980)
4. K. Chandra and G.R. Purdy, *J. Appl. Phys.*, 39 , 2176 (1968)
5. G.D. Sandrock, A.J. Perkins and R.F. Heheman, *Metall. Trans.*, 2 , 2769 (1971)
6. K. Otsuka, T. Sawamura and K. Shimizu, *Phs. Stat. Sol.*, 5 , 457 (1971)
7. P. Moine, G.M. Michal and R. Sinclair, *Acta Metall.*, 30 , 109 (1982)
8. C.M. Hwang, M. Meichle, M.B. Salamon and C.M. Wayman, *Phil. Mag. A*, 47 , No.1, 9 (1983)
9. C.M. Hwang, M. Meichle, M.B. Salamon and C.M. Wayman, *Ibid.*, 47 , No.1, 31 (1983)
10. C.M. Hwang, M. Meichle, M.B. Salamon and C.M. Wayman, *Ibid.*, 47 , No.2, 177 (1983)
11. C.M. Hwang and C.M. Wayman, *Scripta Met.*, 17 , 385 (1983)
12. C.M. Hwang and C.M. Wayman, *Ibid.*, 17 , 1345 (1983)
13. C.M. Hwang and C.M. Wayman, *Ibid.*, 17 , 1449 (1983)
14. C.M. Hwang and C.M. Wayman, *Acta Metall.*, 32 , 183 (1984)
15. C.M. Hwang and C.M. Wayman, *Metall. Trans. A*, 15A , 1155 (1984)
16. P. Bak and V.J. Emery, *Phys. Rev. Lett.*, 36 , 978 (1976)
17. G.J. Tatlock, *Inst. Phys. Conf.*, No.36, 161 (1977)
18. J.A. Wilson, F.J. DiSalvo and S. Mahajan, *Adv. Phys.*, 24 , 117 (1975)

10-10-10

10-10-10

10-10-10

10-10-10

10-10-10

10-10-10

10-10-10

10-10-10

10-10-10

10-10-10

10-10-10

10-10-10

10-10-10

10-10-10

10-10-10

10-10-10

10-10-10

10-10-10

10-10-10

10-10-10

10-10-10

10-10-10

10-10-10

10-10-10

10-10-10

10-10-10

10-10-10

19. T. Honma, M. Matsumoto, Y. Shugo, M. Nishida and I. Yamazaki, Titanium Science and Technology, R. Jaffe ed., 3, 1455 (1980)
20. T. Suburi, T. Tatsumi and S. Nenno, 'ICOMAT 82', 261 (1982)
21. M. Nishida and T. Honma, Scripta Met., 18, 1293 (1984)
22. M. Nishida and C.M. Wayman, Ibid., 19, 983 (1985)
23. Z. Nishiyama, 'Martensitic Transformation', M.E. Fine, Meshii, and C.M. Wayman ed., 263. (1978)
24. K.A. Thornburg, D.P. Dunne and C.M. Wayman, Met. Trans., 2, 2302 (1971)
25. P. Moine, E. Goo and R. Sinclair, 'ICOMAT 82', 243 (1982)
26. G. R. Purdy and J. Gordon Parr, TMS-AIME Trans., 221, 636 (1965)
27. P. Duwez and J. L. Taylor, Trans. AIME., 188, 1173 (1950)
28. E. Hornbogen, Acta Metall., 33, 595 (1985)
29. J. E. Hanlon, S.R. Butler and R.J. Wasilewski, TMS-AIME Trans., 239, 1323 (1967)

MICHIGAN STATE UNIVERSITY LIBRARIES



3 1293 03062 2496